(2)

TECHNICAL REPORT BRL-TR-3206

BRL

TEMPERATURE SENSITIVITY IN ARTILLERY CHARGE DESIGN

RONALD D. ANDERSON
ROBERT T. PUHALLA

FEBRUARY 1991

U.S. ARMY LABORATORY COMMAND

BALLISTIC RESEARCH LABORATORY
ABERDEEN PROVING GROUND, MARYLAND

DISCLAIMER NOTICE

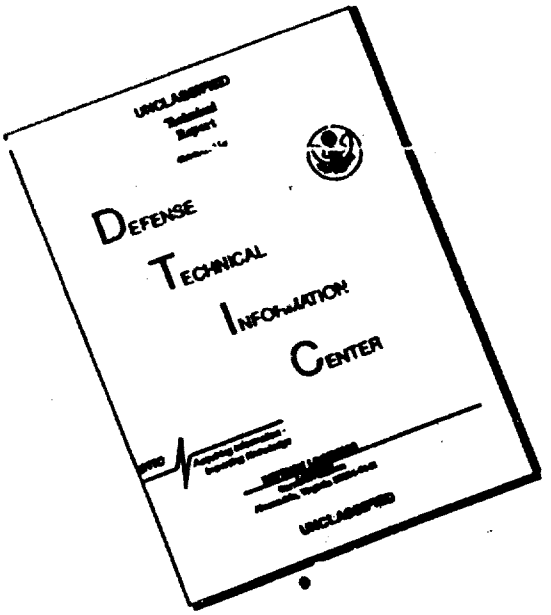

THIS DOCUMENT IS BEST QUALITY AVAILABLE. THE COPY FURNISHED TO DTIC CONTAINED A SIGNIFICANT NUMBER OF PAGES WHICH DO NOT REPRODUCE LEGIBLY.

NOTICES

Destroy this report when it is no longer needed. DO NOT return it to the originator.

Additional copies of this report may be obtained from the National Technical Information Service, U.S. Department of Commerce, 5285 Port Royal Road, Springfield, VA 22161.

The findings of this report are not to be construed as an official Department of the Army position, unless so designated by other authorized documents.

The use of trade names or manufacturers' names in this report does not constitute indorsement of any commercial product.

UNCLASSIFIED

REPORT DOCUMENTATION PAGE

Form Approved
OMB No. 0704-0188

1. AGENCY USE ONLY (Leave blank)	2. REPORT DATE	3. REPORT TYPE AND DATES COVERED
	February 1991	Final Feb 89 - Dec 90

4. TITLE AND SUBTITLE

Temperature Sensitivity in Artillery Charge Design

5. FUNDING NUMBERS

P: 1L161102AH43

6. AUTHOR(S)

Ronald D. Anderson and Robert T. Puhalla

7. PERFORMING ORGANIZATION NAME(S) AND ADDRESS(ES)

8. PERFORMING ORGANIZATION REPORT NUMBER

9. SPONSORING MONITORING AGENCY NAME(S) AND ADDRESS(ES)

USA Ballistic Research Laboratory
ATTN: SLCBR-DD-T
Aberdeen Proving Ground, MD 21005-5066

10. SPONSORING / MONITORING AGENCY REPORT NUMBER

BRL-TR-3206

11. SUPPLEMENTARY NOTES

12a. DISTRIBUTION AVAILABILITY STATEMENT

Approved for Public Release - Distribution Unlimited

12b. DISTRIBUTION CODE

13. ABSTRACT *(Maximum 200 words)*

Charge design for large-caliber artillery weapons must allow for many factors which can reduce efficiency and safety when these rounds are used in field situations. One of those factors is the temperature sensitivity of propellant - the change in performance caused by differing initial charge temperatures in otherwise identical artillery rounds.

By comparing computer simulations of interior ballistic calculations, three factors in propellant grain design are explored - geometry, deterrent layers and ignition delay. The IBHVG2 code is used to show the effects of each factor in a typical 120-mm gun system. Temperature-related trends are computed, and the results are compared in tables and graphs.

14. SUBJECT TERMS

temperature sensitivity; charge design; interior ballistics; IBHVG2; deterrent layer; ignition delay; propellant grains; propellant design; grain geometry

15. NUMBER OF PAGES

48

16. PRICE CODE

17. SECURITY CLASSIFICATION OF REPORT	18. SECURITY CLASSIFICATION OF THIS PAGE	19. SECURITY CLASSIFICATION OF ABSTRACT	20. LIMITATION OF ABSTRACT
UNCLASSIFIED	UNCLASSIFIED	UNCLASSIFIED	SAR

TABLE OF CONTENTS

THIS PAGE INTENTIONALLY LEFT BLANK.

LIST OF FIGURES

THIS PAGE INTENTIONALLY LEFT BLANK.

LIST OF TABLES

THIS PAGE INTENTIONALLY LEFT BLANK.

1. INTRODUCTION

The goal of large-caliber ballistic technology is not only to send a projectile far and fast, but also to send it to a particular location. Speed and distance are desired, but accuracy is essential. There are many factors within a gun system which can affect accuracy; as each factor is researched, understood, and controlled, then the modified gun system becomes more efficient in consistently placing its projectile on the target.

The perfect solution for artillery is to launch a projectile at a precise velocity in order to achieve first-round accuracy, and to avoid overpressures caused by external conditions. This perfect round gives the same projectile velocity under desert heat and arctic cold, at sea level and mountainous terrain, and after long storage periods. Unfortunately, the perfect artillery round does not exist. Shot-to-shot variations in interior pressures and projectile exit velocities are induced by factors too numerous to list. Understanding these factors helps design rounds which will perform consistently and safely under a variety of conditions.

One of those factors to be understood and controlled is temperature sensitivity of the propelling charge. If small temperature changes in the propellant cause large variations in internal gun pressures, then it is likely that similar variations will also be present in projectile exit velocity. Since it is not possible to do all gun firings in a static temperature environment, nor is it practical to pre-condition each round for several days before its firing time, then the effects of temperature-induced pressure and velocity changes must be known before an accurate shot can be made.

The purpose of this report is to explore analytically the trends in temperature sensitivity of large-caliber charges through (1) the role of grain geometry, (2) the effects of a deterrent layer applied to propellant grains, and (3) ignition delay.

2. GUN SYSTEM PARAMETERS

Computer models of interior ballistic equations are a cost-effective method of exploring ballistic concepts. Differences in charge weights or grain design are much easier to show by means of a computer program than to measure artillery breech pressures, or to produce propellant granulations over a range of dimensions.

The calculations for this study were made with the IBHVG2[1] computer code developed at the Ballistic Research Laboratory. A lumped-parameter code, IBHVG2 contains mathematically precise form functions for many propellant geometries. The program can also apply non-uniform layers to the theoretical propellant grains, and keeps track of any and all depth-dependent rheological properties as the grains burn away during the interior ballistic computation.

Since all propellant charges in this study are theoretical, they have all been represented as containing only an igniter and a main charge. Parasitic elements such as combustible cases, flash reducers, and de-coppering agents have not been used. Also, there will be no minimum or maximum in loading density -- all charges are considered possible, including those whose dimensions could exceed the chamber walls in one or more directions. The purpose of this study is to look for definable trends in temperature sensitivity, not to design realistic propellant charges.

A 120-mm gun system was chosen for modeling purposes. Those parameters which remained constant throughout the calculations are shown in Table 1. The propellant data in Table 2 were taken from a closed-bomb investigation of burning rates for a JA2 propellant;[2] thermodynamic properties were computed by the BLAKE code.[3] The 21° C (494° K) set of burning rates will hereafter be referred to as the "ambient" rate, while the 49° C (522° K) rates will be "hot." Sample input decks are shown in the Appendices of this report.

Table 1. Gun System Parameters.

Bore Diameter	*120 mm*
Smoothbore	
Chamber Volume	*9210 cc*
Projectile Weight	*9.525 kg*
Projectile Travel	*4.7498 m*
Igniter (Black Powder)	*0.1 kg*
Pressure Gradient	*Pidduck-Kent*

Table 2. Propellant Information.

Type	*JA2 Lot 792-2*
Density	*1.60 g/cc*
Covolume	*0.938 cc/g*
I B Gamma	*1.2247*
Force	*1143.2 J/g*
Flame Temp	*3558 °K*

Burning Rates		
Pressure (MPa)	21 °C Rate (cm/s)	49 °C Rate (cm/s)
68.95	7.63	8.11
137.89	13.83	14.70
206.84	20.34	21.10
275.79	26.26	28.32

3. PROPELLANT GRAIN GEOMETRY

Temperature sensitivity of a propelling charge can be defined as the difference in performance when identical rounds are fired after being stored at unequal temperatures, and can easily be seen in terms of maximum internal gun pressures or projectile exit velocities. The pressure difference is due to a (usually) faster burning rate at higher initial temperatures, causing a more rapid pressurization in the early part of the ballistic cycle. When internal pressures are raised, the projectile is accelerated faster, and exit velocity increases.

As an example, observe the results of two simulated firings of a single-perforated (1-perf) propellant charge (Figure 1). The first computation uses ambient (21° C) burning rates, and the second uses the same propellant parameters except for the hot burning rate. The ambient results give a maximum breech pressure of 500.0 MPa and projectile exit velocity of 1439 m/s, while the hot rates produce 614.1 MPa maximum

breech pressure and 1564 m/s velocity. If one uses the difference in maximum breech pressures as a measure of temperature sensitivity, then the pressure difference (ΔP) is 114.1 MPa.

Figure 1. Temperature-Induced Breech Pressure Differences.

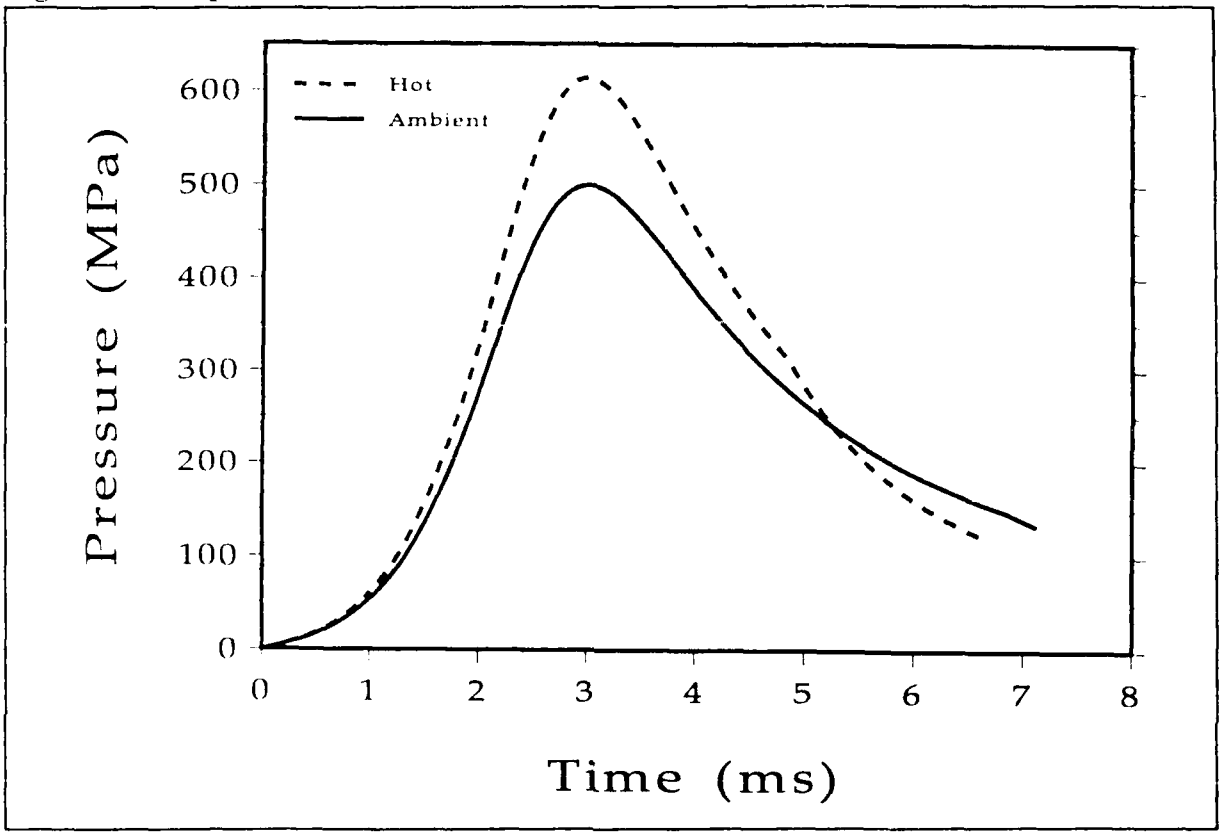

The geometry of propellant grains can play a significant part in determining the amount of temperature sensitivity for any given charge. Maximum breech pressures were compared for a series of grain geometries: spherical; rolled Ball Powder® propellant (made by "squashing" a spherical grain into a pancake shape); and singie-, seven-, and nineteen-perforated cylinders. Multi-perforated grain forms are the most progressive-burning of the five geometries -- that is, they have more surface available for burning as the ballistic cycle advances. The expanding area inside the perforations more than compensates for the loss of exterior surface area, until the perforations burn through to each other (called "slivering") -- then available surface area rapidly decreases. Spherical propellant grains are the most regressive of the five geometries -- available surface area is greatest at the time of ignition, and decreases monotonically as the grain burns away.

For this comparison, charges were designed with each grain geometry to obtain a 500 MPa maximum breech pressure (P_{MAX}) at ambient burning rates. Each charge contained 8.5 kilograms of propellant, so that total energy within the systems remained

Note: Ball Powder® is a registered trademark of Olin Corporation.

constant. One grain dimension was varied at ambient temperature in order to achieve desired P_{MAX} pressure. In perforated-grain cases, web was changed; for the spherical grain, obviously, diameter varied; in the rolled-ball cases, thickness was the alterable dimension.

A rolled-ball major diameter of 9 millimeters was chosen for this study. In this instance the diameter is approximately three-and-one-half times the thickness -- somewhere in the mid-range between the regressive spherical geometry and the nearly constant-area single-perf grain. A spherical grain has a diameter-to-thickness ratio of identically one, while a much larger (>10) ratio is similar to a constant-surface-area geometry.

Also, for all perforated grains, the perforation diameters (0.762 mm) and grain lengths (0.5 meters, in order to decrease end-area effects) were kept constant to ease the comparison process. The results in some cases may not necessarily be the optimum charge design, but the trends should remain true.

Figure 2 is a graph of the breech pressure versus ballistic time curves of the most regressive, nearly neutral, and most progressive grain geometries. The single-variable grain dimensions were allowed to change so that an 8.5-kg propellant charge would produce a 500-MPa P_{MAX} pressure. The sharp break in the 19-perf data shows where slivering has taken place. Now using the same grain dimensions, insert the "hot" burning rates, and the pressure-time curves change to those in Figure 3. Though all pressures increase with the higher burning rates, the progressive (19-perf) geometry increases most, and the spherical-grain charge increases least.

Table 3. Constant-Energy Geometry Calculations.

Geometry	Ambient			Hot			
	P_{MAX} (MPa)	Time (ms)	Travel (cm)	P_{MAX} (MPa)	Time (ms)	Travel (cm)	ΔP (MPa)
Sphere	500	2.692	26.70	588	2.634	28.50	88
Rolled-Ball *	500	2.771	28.48	594	2.721	30.95	94
1-Perf †	500	3.000	34.12	614	2.986	39.60	114
7-Perf †	500	3.572	51.32	682	3.753	76.14	182
19-Perf †	500	3.977	66.29	724	3.950	78.92	224

Notes: * Diameter/Thickness Ratio $\simeq$ 3.5
† Length = 0.5 m

Table 3 compares breech pressure maximums for the two temperatures and the five modeled geometries. Charge weights have been kept at 8.5 kg JA2 propellant in all cases. The column labelled **Time** refers to the computed ballistic time of the maximum pressure event, and **Travel** is projectile displacement at the time of pressure maximum. The progressive-geometry grains show wider fluctuations in pressure due to temperature-based burning rate variations. The column labeled **ΔP** is the pressure difference between "hot" and "ambient" cases, and is a convenient measure of

Figure 2. Breech Pressures at Ambient Temperature.

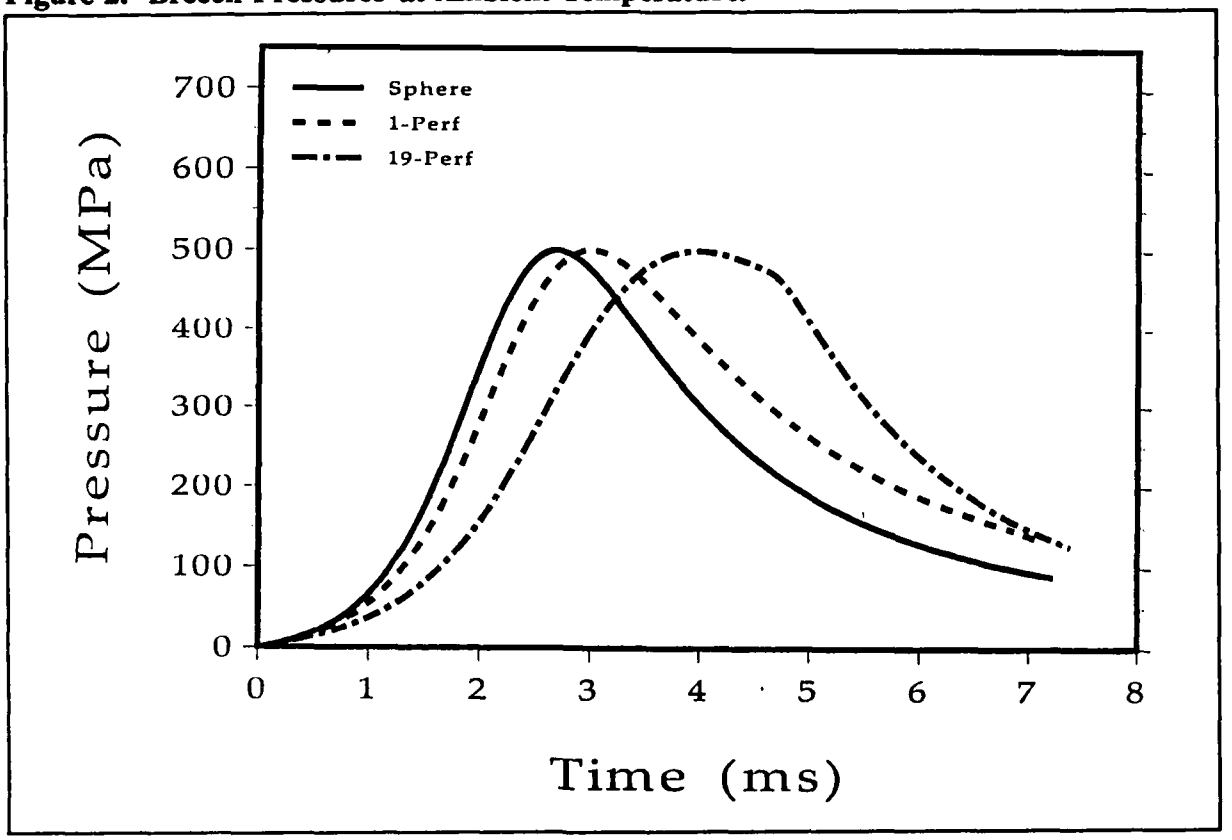

Figure 3. Breech Pressures at Hot Temperature.

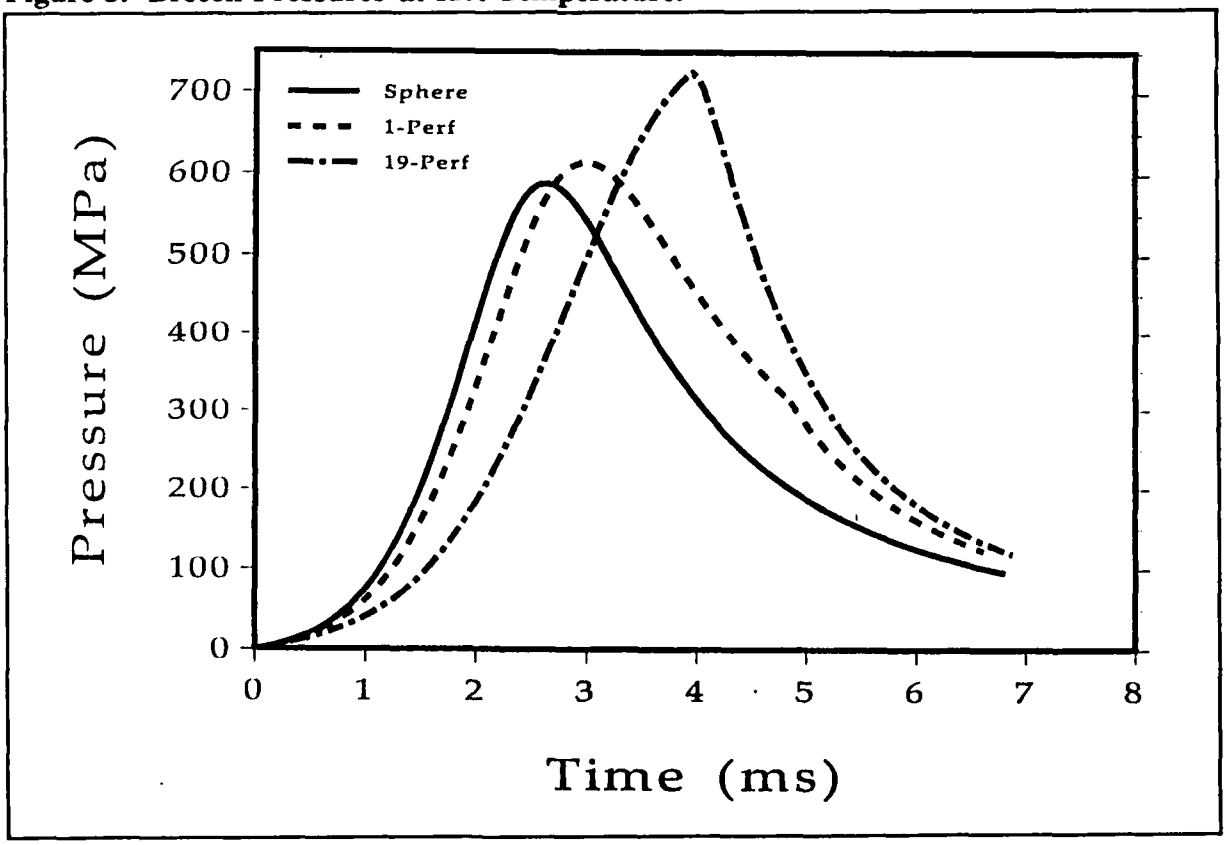

temperature sensitivity. Note also that projectile travel at the time of P_{MAX} increases with progressivity.

Equal charge weights easily show the differences grain geometry makes when burning rates are varied, but the study of grain shape versus temperature sensitivity need not be constrained by weight. One of the very real limitations imposed on gun systems is the maximum pressure that the chamber and tube can safely withstand.

Charges are often designed to take advantage of the highest pressure limit acceptable by the gun tube. One can find a "most efficient" grain design for a series of charge weights at ambient temperatures, then apply the hot burning rates to test those weight/dimension combinations against the maximum tube design pressure (662 MPa at breech). In this study, a four-step iterative process was chosen for grain design optimization. The steps are:

1. Choose a maximum breech pressure for ambient conditions
2. Find the charge-weight and web combination giving highest velocity
3. Try this combination with the hot burning rates
4. Iterate with higher/lower pressures in Step 1. until Step 3. produces a P_{MAX} consistent with the gun tube limitation

Tables 4 and 5 show part of the optimization study of the rolled-ball example. For Table 4, the ambient breech pressure maximum was 551.6 MPa, projectile exit velocity peaked at a charge weight of 6.9 kg and a grain thickness of 2.467 mm. Table 5 is from the calculations for 568.8 MPa, where velocity reached a maximum at a charge weight of 6.95 kg and grain thickness of 2.444 mm. This study varied ambient P_{MAX} from 551.6 MPa to 568.8 MPa in five equal steps, and charge weights were varied in increments of 0.05 kg.

Table 4. Optimization Calculations.

Chg Wt (kg)	Thick (mm)	P_{MAX} (MPa)	Vel (m/s)
6.7500	2.3339	551.59	1433.3
6.8000	2.3771	551.59	1433.8
6.8500	2.4214	551.59	1434.0
6.9000	2.4667	551.59	1434.1
6.9500	2.5131	551.59	1433.9
7.0000	2.5606	551.59	1433.3
7.0500	2.6093	551.59	1432.4
7.1000	2.6593	551.59	1431.2
7.1500	2.7106	551.59	1429.6
7.2000	2.7632	551.59	1427.6

Table 5. Optimization Calculations.

Chg Wt (kg)	Thick (mm)	P_{MAX} (MPa)	Vel (m/s)
6.7500	2.2720	568.83	1444.5
6.8000	2.3136	568.83	1445.3
6.8500	2.3562	568.83	1446.1
6.9000	2.3998	568.83	1446.6
6.9500	2.4444	568.83	1447.0
7.0000	2.4900	568.83	1446.9
7.0500	2.5369	568.82	1446.6
7.1000	2.5848	568.83	1446.0
7.1500	2.6340	568.83	1445.2
7.2000	2.6845	568.83	1443.8

Figure 4 is a graph of those charge-weight/web combinations plotted against computed projectile exit velocity. When drawn over a band of pressure solutions, the charge weight versus velocity curves are a series of arcs which peak at the most efficient grain geometry for each target pressure. Applying those "peak efficiency" points to the gun system using the high-temperature burning rates will cause the model to arrive at a series of higher maximum breech pressures (Table 6). In this case the grain design which was found at a 555.0 MPa ambient pressure comes very close to the gun tube design pressure for the "hot" system -- and the grain geometry and charge weight which produced this result would be chosen as the optimum combination.

Figure 4. Projectile Exit Velocities.

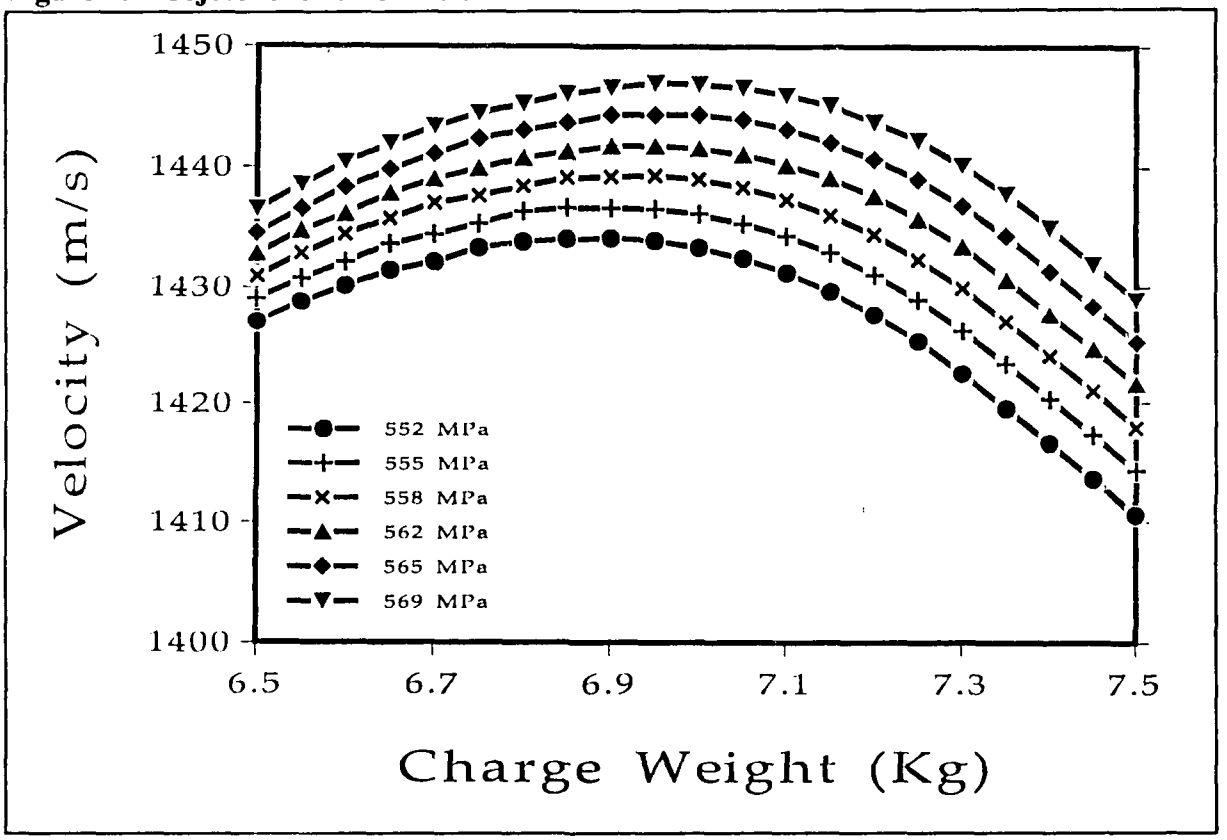

Table 6. Peak Charge-Weight/Dimension Calculations.

Ambient				Hot	
Maximum Breech Press (MPa)	Projectile Exit Vel (m/s)	Charge Weight (Kg)	Grain Thickness (mm)	Maximum Breech Press (MPa)	Projectile Exit Vel (m/s)
551.6	1434.1	6.90	2.4667	656.7	1495.0
555.0	1436.6	6.90	2.4529	661.5	1497.3
558.5	1439.3	6.95	2.4850	666.5	1502.2
561.9	1441.8	6.95	2.4713	671.3	1503.5
565.4	1444.4	6.95	2.4577	676.2	1506.5
568.8	1447.0	6.95	2.4444	681.1	1507.8

Using the same procedure for the other grain geometries, a table of "best designs" was created for the five systems (Table 7). All geometries are optimized at ambient pressures. Charge weights and grain dimensions shown are those combinations which produce "hot" pressure maximums closest to the gun tube limitation. Position in centimeters refers to projectile travel at the time of "hot" pressure maximum. As expected, the progressive grains show greatest pressure differential; the rolled-ball and spherical geometries are least temperature sensitive.

A velocity comparison between the geometries shows that the more progressive grains are able to put more propellant into the chamber and more energy into projectile velocity, while still staying within maximum tube pressure limitations at the high-temperature calculations. The regressive grain types, due to the greatest surface area early in the ballistic cycle, reach limiting pressures much quicker in the calculations and must keep charge weights down in order to stay within pressure limits.

Table 7. Optimized Geometry Comparison.

Geometry	Chg Wt (kg)	Ambient P_{MAX} (MPa)	Ambient Vel (m/s)	Hot P_{MAX} (MPa)	Hot Vel (m/s)	Hot Travel (cm)	ΔP (MPa)
Sphere *	6.95	565.4	1383	662.6	1449	28.50	97.2
Rolled-Ball †	6.90	555.0	1437	661.5	1497	33.56	106.5
1-Perf ‡	7.95	529.2	1489	661.3	1577	44.05	132.1
7-Perf ‡	8.85	486.8	1518	662.5	1629	75.64	175.7
19-Perf ‡	9.35	460.6	1516	661.8	1644	103.50	201.2

Notes:
* Burned at exit: 6.45 kg Ambient, 6.71 kg Hot
† Major Diameter = 9.0 mm ; Diameter/Thickness $\simeq$ 3.5
‡ Length = 0.5 m ; Perf Diam = 0.762 mm

The charge weight data point shown here for spherical propellant may be slightly misleading because of incomplete combustion during the ballistic cycle. The optimization process did not require an "all-burnt" consideration for charge design. Rolled-ball and single-perf charges burned completely in both ambient and hot design stages; the 7- and 19-perf grains typically show their ambient velocity peak when less than one percent remains unburnt in the tube, and the hot-temperature cases burned completely. However, the ball-propellant case here burned only 93% at projectile exit in the ambient calculation, and 97% in the hot-temperature calculation. If the table here showed "charge weight burned" instead of "initial charge weight," then the value for the hot-rate spherical case would be 6.714 kg.

The progressive geometries show more pressure difference between ambient and hot temperature models -- meaning a higher temperature sensitivity and need for closer temperature monitoring in order to predict projectile exit velocities and trajectories. But these multi-perforated grain charges also result in higher velocities than the other three grain types. The regressive-grain charges, because of lower temperature variability, will provide a lower dispersion due to temperature differences. In an actual design situation

for artillery, where propellant temperatures may not be well-known, choosing grain types and dimensions could be a trade-off between system accuracy and maximum range.

Figure 5 is a graph of the relative burning surface area versus time from the ambient-temperature optimized grains. Each curve has been normalized by dividing the current surface area by its initial (pre-burning) surface value. The 1-perf curve remains near a value of 1.0 until propellant burnout; this corresponds to a near-neutral progressivity. The 7-perf curve rises to a peak value of 1.92, then falls away as the remaining grain slivers burn out. Progressivity of the 19-perf grain is even higher, reaching a value of 2.53 for *S/S0*. Spherical grains are the least progressive geometry, and rolled-ball propellant grains (width-to-thickness ratio of approximately 3.5) fall between spherical and 1-perf curves.

Figure 5. Normalized Surface Area During Grain Burning.

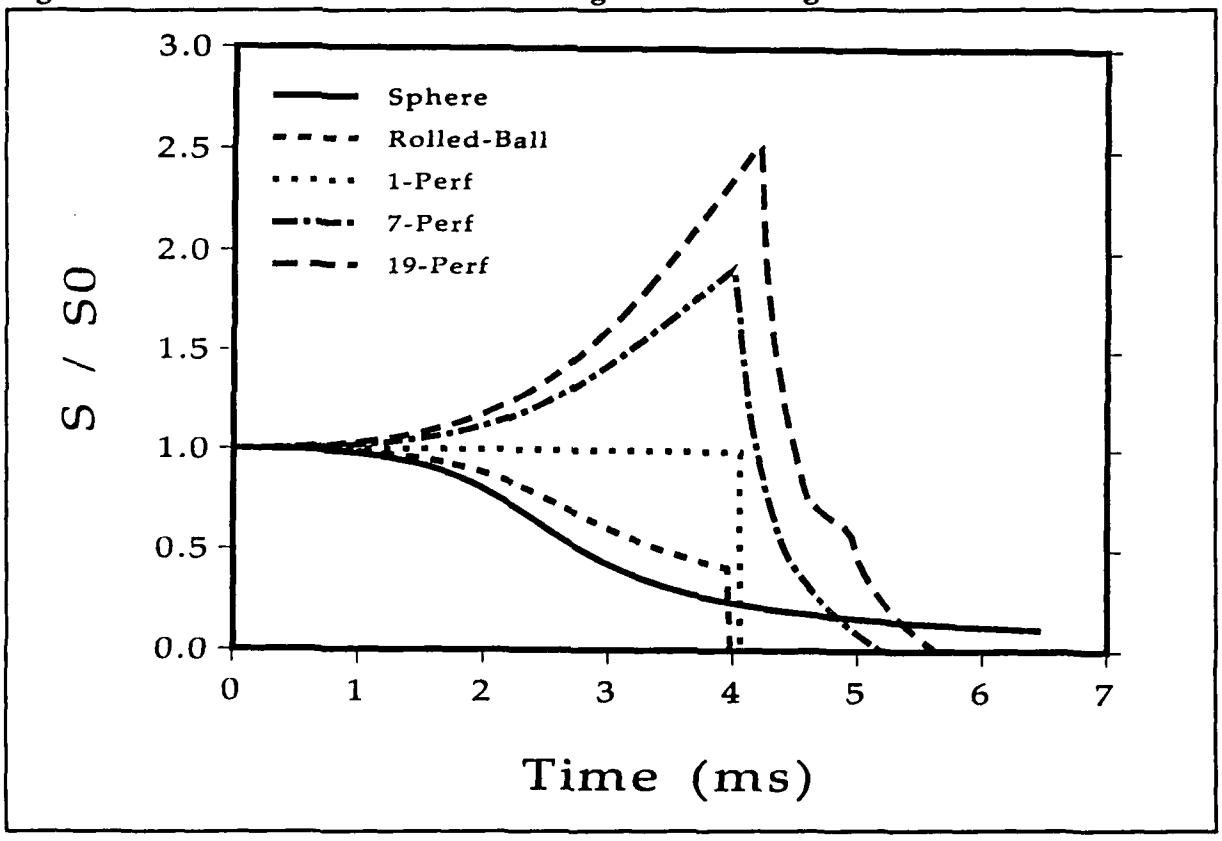

Delaying the position of the maximum pressure event is very important because it directly affects projectile velocity. The peak pressure event in the gun system can be interpreted as the moment when propellant burning rate has been overcome by an increase in available volume -- the projectile is moving so fast (allowing more of the gun tube to be used for gas expansion) that the newly produced gas cannot sustain a pressure increase. Once base pressure starts dropping, projectile acceleration also falls. The connection between acceleration and velocity in the present gun system, for example, can be explored through two simplified equations. When F is the force (pressure) on the projectile base, then $F = ma + L$ where m is projectile mass, a is acceleration, and L is

Figure 6. Base Pressures versus Projectile Travel.

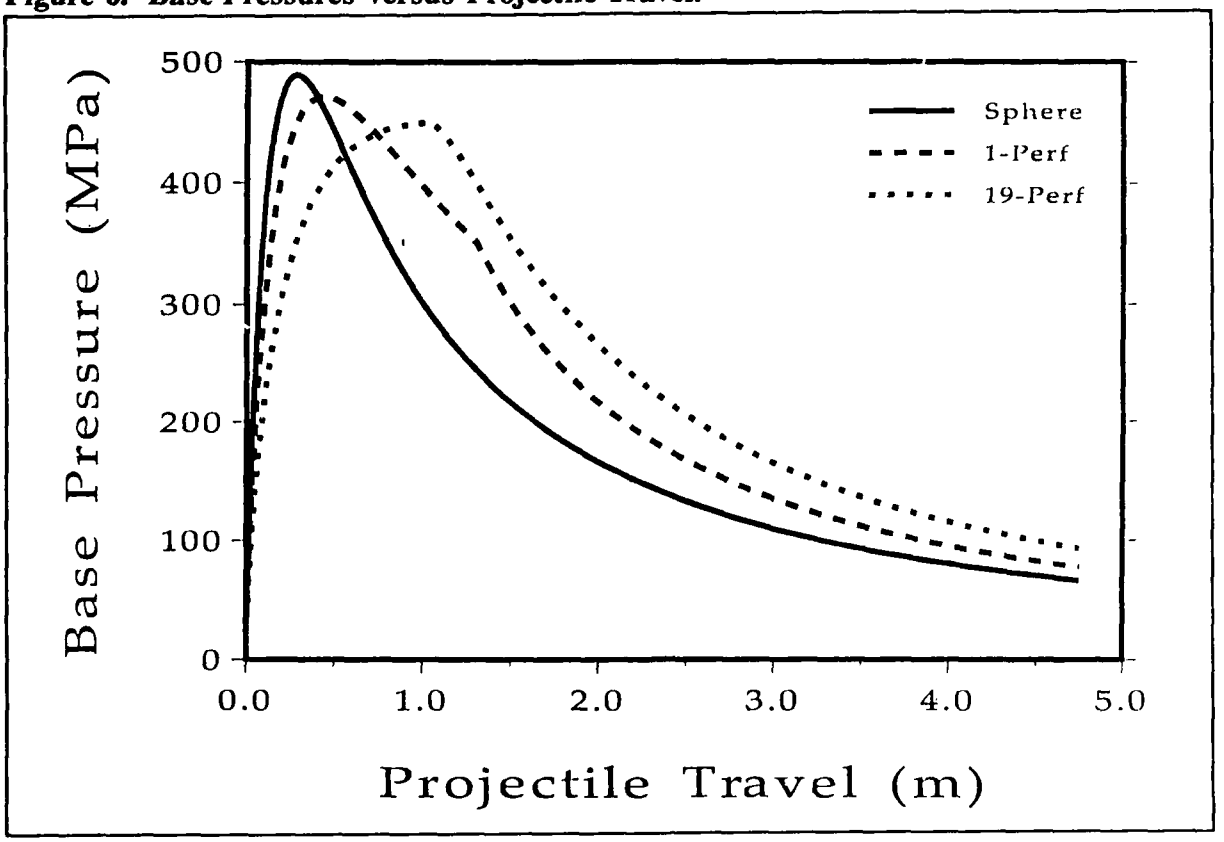

Figure 7. Acceleration versus Projectile Travel.

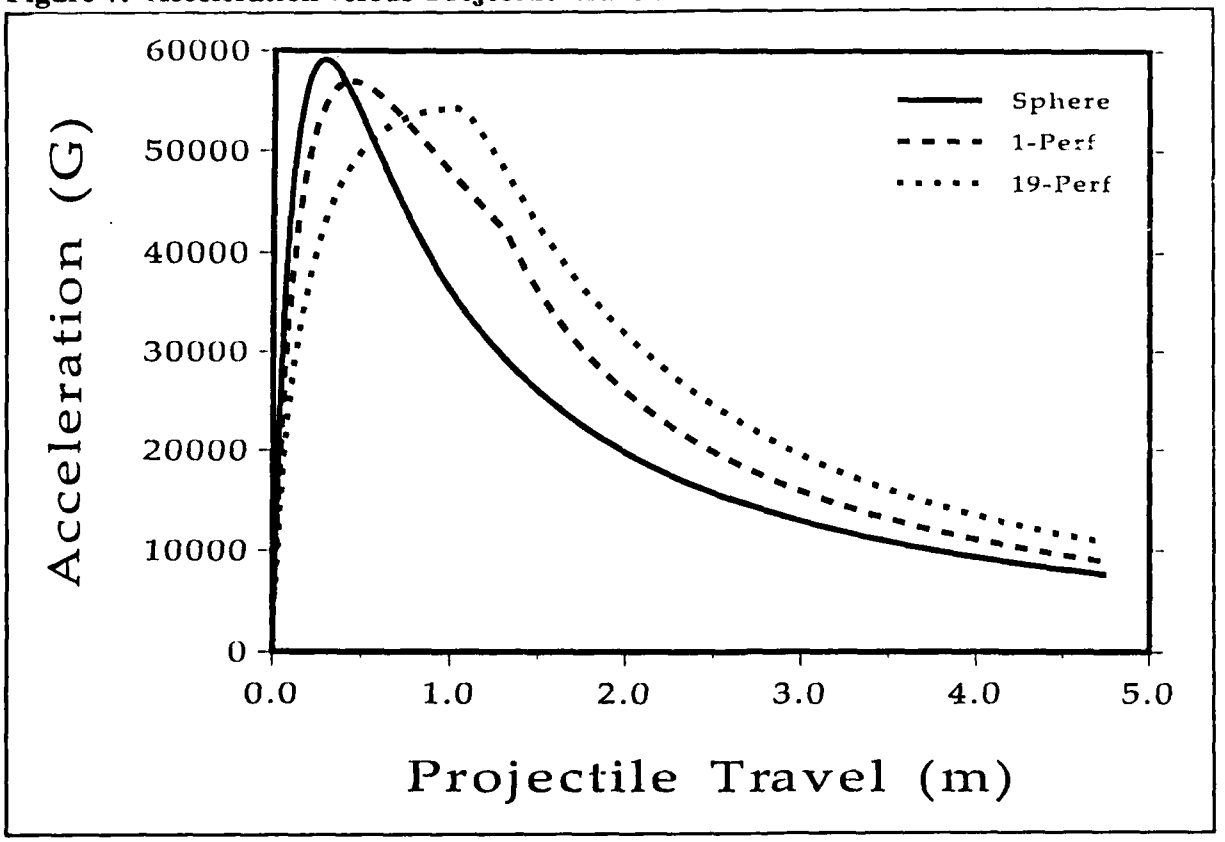

a loss term due to bore resistance or friction. (No energy is lost to rotational forces because a smoothbore is being modeled, and air resistance differences in front of the projectile are assumed to be negligible.) The energy imparted to the projectile can be represented as $\int F$ over distance, or $\int(ma + L)$, where $\int ma$ is kinetic energy and $\int L$ is energy lost as friction (heat) to the gun tube wall and to the obturator. Since the bore resistance does not change due to propellant grain type, the integral of L may be assumed a constant for this gun system. Projectile kinetic energy may also be defined as $KE = \frac{1}{2}mv^2$, so v^2 is proportional to $\int a$.

Figure 6 is a graph of data taken from the computations which produced Table 7. The "hot" data for spherical, single-perf, and 19-perf granular charges created the three curves of projectile base pressure versus projectile travel. The IBHVG2 inputs include a Pidduck-Kent pressure gradient model, which relates breech and base pressures to the calculated mean pressure. Though all three maximum breech pressures were 662 MPa, the maximum base pressures differ because of the distance the projectile had travelled from charge ignition to time of P_{MAX}. Base pressure curves are almost identical to acceleration curves (Figure 7), and the total area under the acceleration curve is proportional to energy transferred to the projectile. By inspection, the 19-perf curve shows highest total energy transfer due to retention of a higher base pressure. (The sharp break in the 1-perf curve corresponds to propellant burnout).

4. DETERRENT LAYER

A deterrent layer is often added to propellant grains in order to tailor the rate of gas production. It is usually done to lower the propellant burning rate on and near the outer surface. The use of deterrents is based on the same principle as progressive geometry -- to produce maximum pressures later in the ballistic cycle. This layer may be deposited in one of two methods -- either by "painting" the grain with a dissimilar outer coating, or by chemically altering the composition of the existing outer portion.

The "paint" method results in an outer layer of uniform consistency as far as thermodynamic properties are concerned -- molecular weight, burning temperature, covolume, etc. The additional material may be added by dipping grains in an adhering solution, and timing the process so that a desired thickness of the new material will be present when the dipping is finished. Several coatings could be formed by repeating this process with other energetic solutions. Varying the properties and thicknesses of these layers can provide a great deal of control over the rate and timing of gas production during the ballistic cycle.

Chemical processing can form a varying-property layer over the grain surface. If solvents and/or solutions can be found to react on a molecular level with the base propellant, then an outer layer can be formed which may have depth-dependent thermodynamic parameters. The base grain can be immersed in the reacting liquid for a measured time -- the rate of physical penetration of the liquid into the base propellant controls the depth of the reaction. Since the outermost portion of the original grain has

Figure 8. Cross-sectional Profile of Deterred Rolled-Ball Grain.

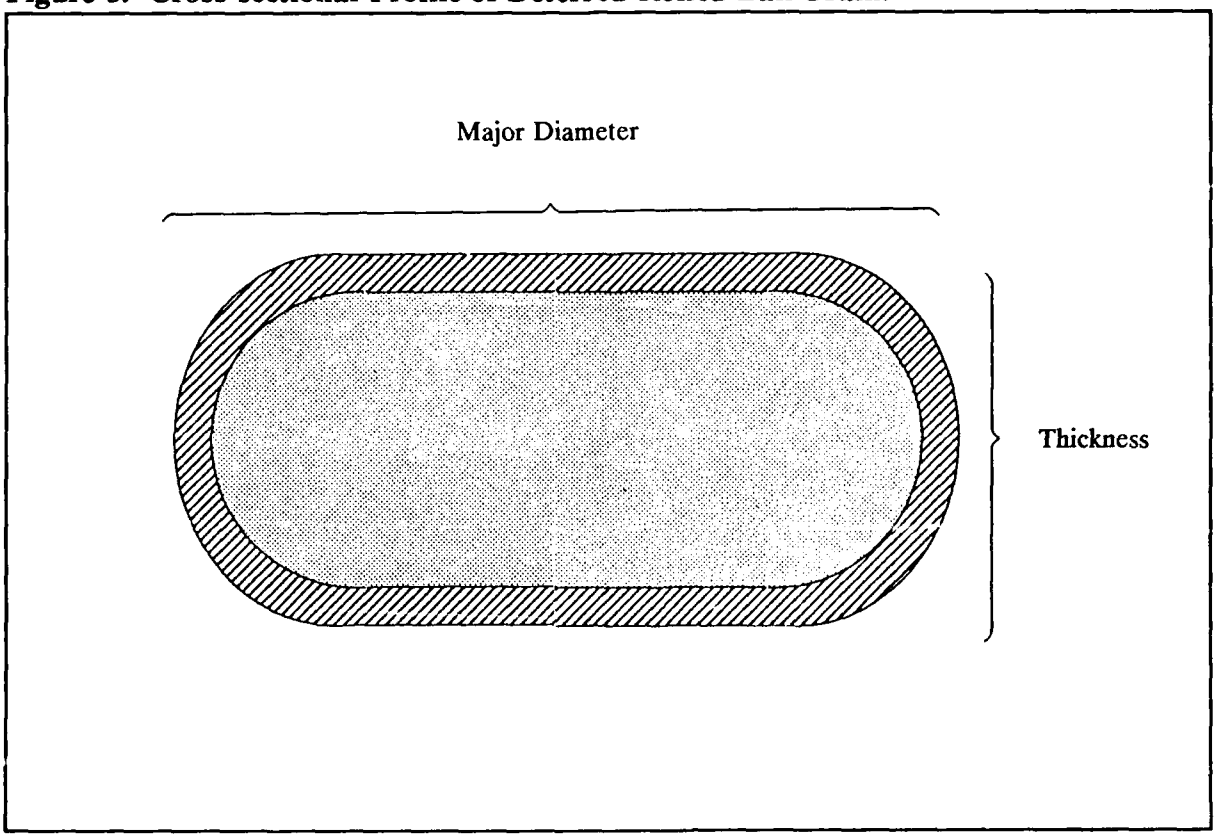

Figure 9. Burning Rates as Function of Depth from Grain Surface.

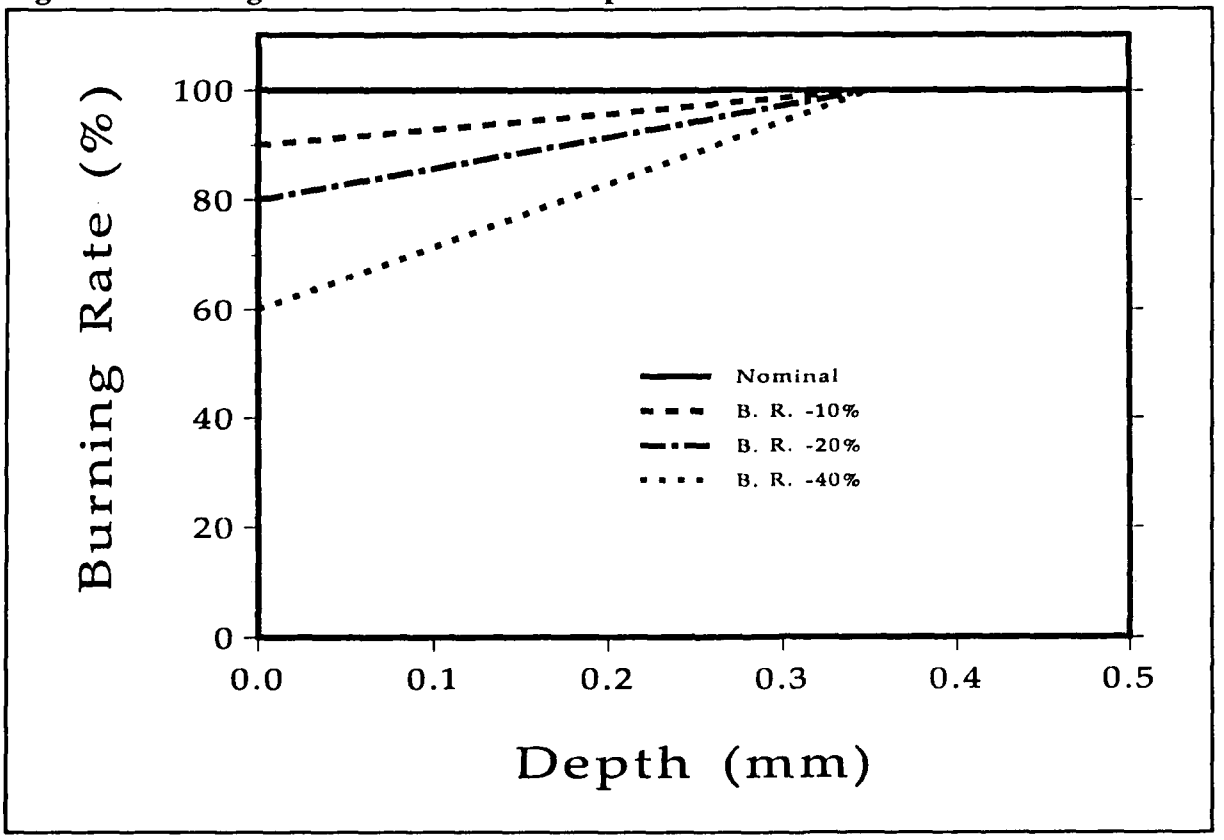

had most exposure to the solution, it may show the most change from base-grain properties. As depth increases, a difference will still be evident until the limit of penetration is reached, where the base propellant is unchanged from its original state. The amount of thermodynamic difference from base propellant properties may or may not be monotonic in relation to the depth of penetration.

Both of the methods mentioned for deterrent deposition can be applied to a spherical or rolled-ball grain. Perforated grains may pose problems, since inner surfaces are not as easily reached by the "paint" or by the chemical agent.

For this study, we will assume an outer layer of a rolled-ball grain has been chemically deterred. Figure 8 is a drawing of the cross-section of such a theoretical grain, where the deterred layer is represented by a shaded area and the base propellant is unshaded. The outer surface now has a burning rate which is lower than the base grain -- the difference in rate will be represented by a multiplicative factor. The burning rate smoothly returns to normal as one moves toward the center of the grain, and is fully recovered at a point 0.35 millimeters below the surface. The four factors will be 1.0, 0.9, 0.8, and 0.6 - to be referred to as non-deterred (ND), ten-percent reduction (DT10), twenty-percent reduction (DT20), and forty-percent reduction (DT40), respectively. Figure 9 shows a graph of the different burning rate factors versus perpendicular depth into the grain.

This is a conservative representation -- actual deterred layers may have much more burning rate variation and a much steeper profile. Additional differences in flame temperature, molecular weight of gaseous products, and other thermodynamic properties are commonly seen in most deterrent layers. For purposes of this study, we will assume no other thermodynamic properties are affected; only the effect of an altered burning rate will be studied.

The grain for this part of the study will be 1.88 millimeters thick, and will have a major diameter of 2.51 millimeters, for a length-to-thickness ratio of approximately 1.33. This ratio is much closer to a spherical grain than a constant-surface pancake.

Using the same gun system parameters as in the geometry study, one can find a charge weight which will produce a maximum breech pressure of 500 MPa with a non-deterred (ND) grain. Then use the same weight for a 10%-deterred charge, a 20%-deterred charge, and finally apply the forty-percent burning-rate reduction. Figure 10 shows the breech pressure versus ballistic time curves from these calculations. Maximum breech pressures drop as the deterrent level increases. Table 8 shows calculated data from those four cases, where the same charge weight at ND, DT10, DT20, and DT40 burning rates produces progressively lower breech pressures and exit velocities.

If charge weights are increased for the deterred cases so that ambient maximum breech pressures are equal, then the higher loading densities raise velocities -- but also increase temperature sensitivity (Table 9). This is a fairer comparison of temperature

Figure 10. Breech Pressures from Equal Charge-Weight Calculations.

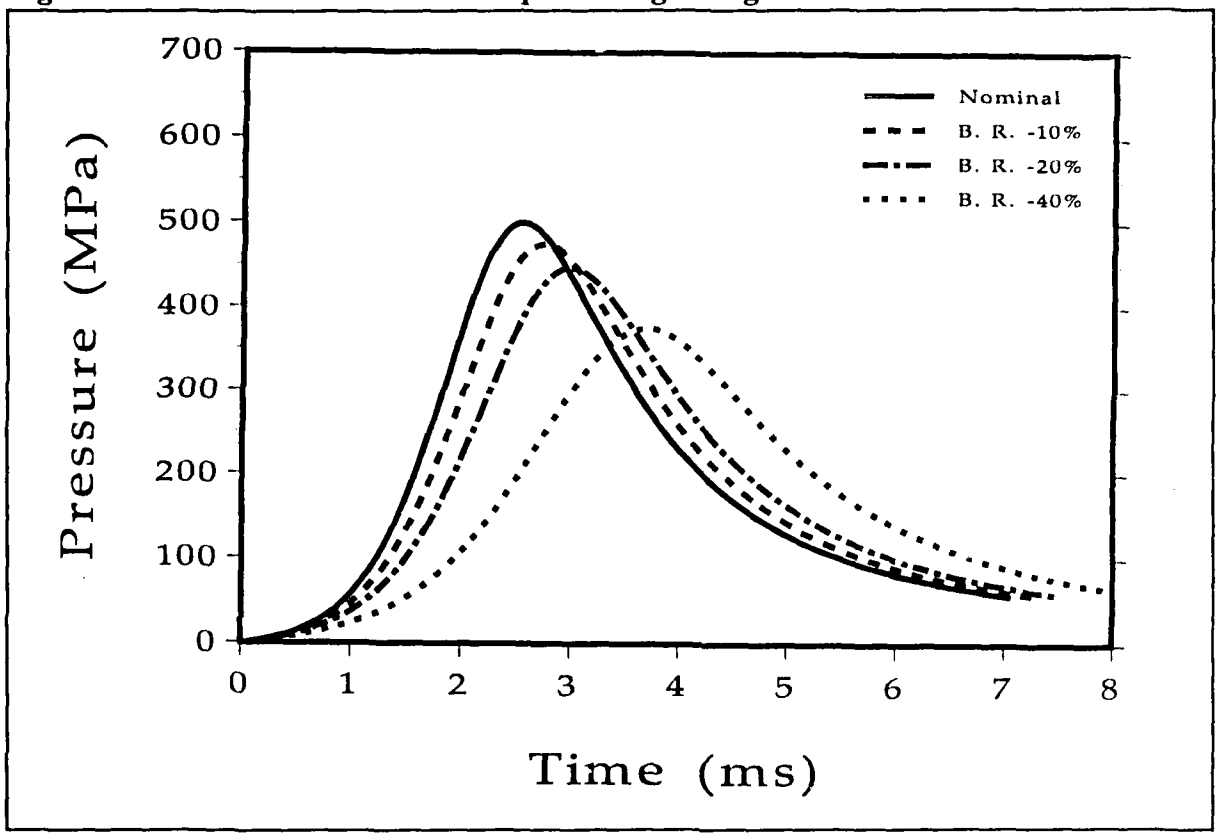

Table 8. Equal Charge-Weight Calculations.

Deterrent %	Chg Wt (Kg)	Ambient Br Pr Max (MPa)	Ambient Vel (m/s)	Hot Br Pr Max (MPa)	Hot Vel (m/s)	ΔP (MPa)
N-D	4.675	500	1258	551	1274	51
10	4.675	475	1250	525	1266	50
20	4.675	447	1240	494	1257	47
40	4.675	375	1209	417	1229	41

Table 9. *Equal Ambient Pressure Maximums.*

Deterrent %	Charge Wt (Kg)	Ambient P_{MAX} (MPa)	Ambient Velocity (m/s)	Hot P_{MAX} (MPa)	Hot Velocity (m/s)	ΔP (MPa)
N-D	4.675	500	1258	551	1274	51
10	4.787	500	1269	555	1286	55
20	4.922	500	1281	559	1300	59
40	5.298	500	1314	571	1337	71

Figure 11. Breech Pressure Histories from 500-MPa Ambient Calculations.

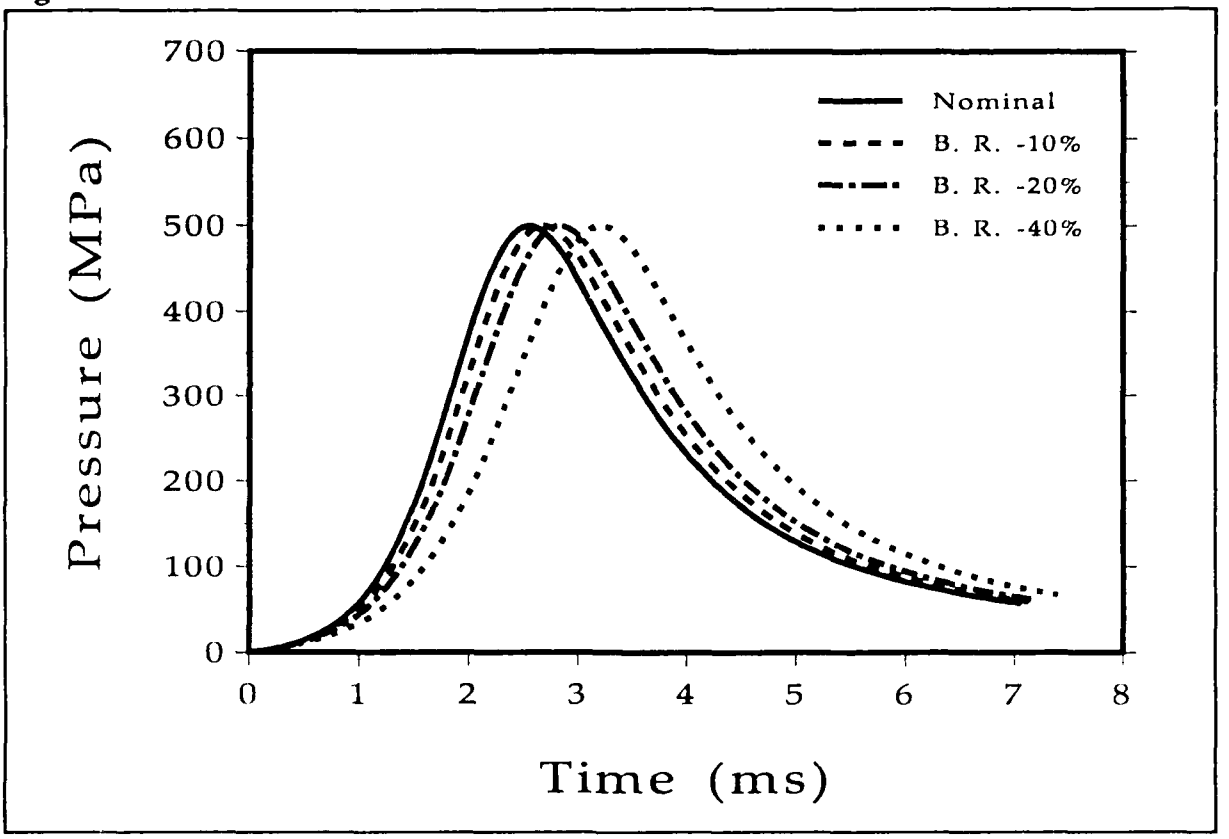

Figure 12. Pressure Histories from Hot Propellant Calculations.

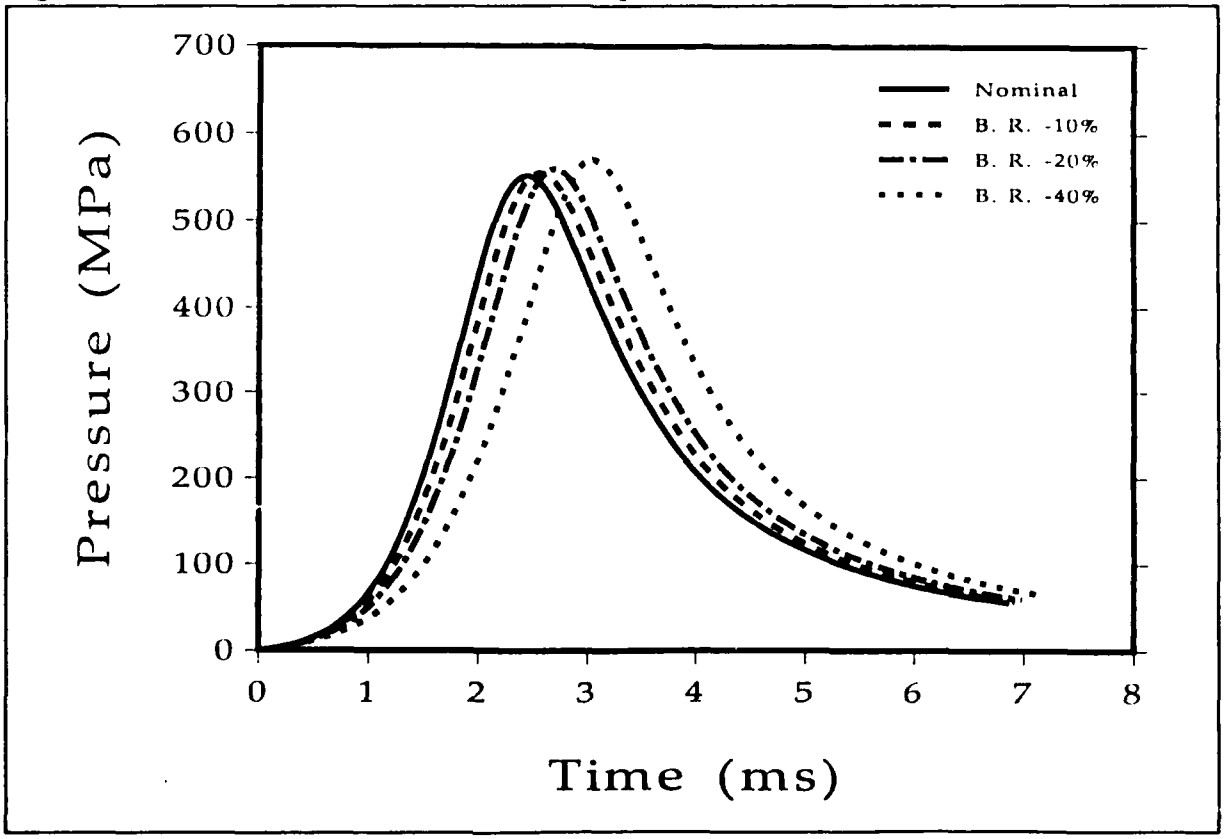

sensitivity, since pressures are equal at one end of the temperature scale. Graphing breech pressures versus time (Figure 11) at ambient temperature shows that higher deterrent levels delay the time of P_{MAX}, as expected. Graphing "hot" cases also shows the increased temperature sensitivity as deterrent strength increases (Figure 12).

Table 10. Equal Hot Pressure Maximums.

Deter %	Charge Wt (Kg)	Ambient P_{MAX} (MPa)	Ambient Vel (m/s)	Hot P_{MAX} (MPa)	Hot Vel (m/s)	Travel (cm)	ΔP (MPa)
N-D	5.049	591	1321	662	1338	21.43	71
10	5.148	588	1329	662	1347	23.02	74
20	5.266	583	1338	662	1358	24.95	79
40	5.596	571	1363	662	1388	30.50	91

If the four deterrent levels are compared when the high-temperature computations are keyed to 662 MPa (maximum pressure limitation from the geometry study), the same trends are evident (Table 10) as deterrent strength increases: higher exit velocities, greater temperature sensitivity. Graphing the breech pressures against time for the "hot" runs also shows that the higher deterrent level again tends to delay the time of maximum pressure events (Figure 13). Table 10 also shows projectile travel (from initial position) at instant of maximum breech pressure.

Figure 13. Pressure History for 9mm-Diameter Rolled-Ball Propellant.

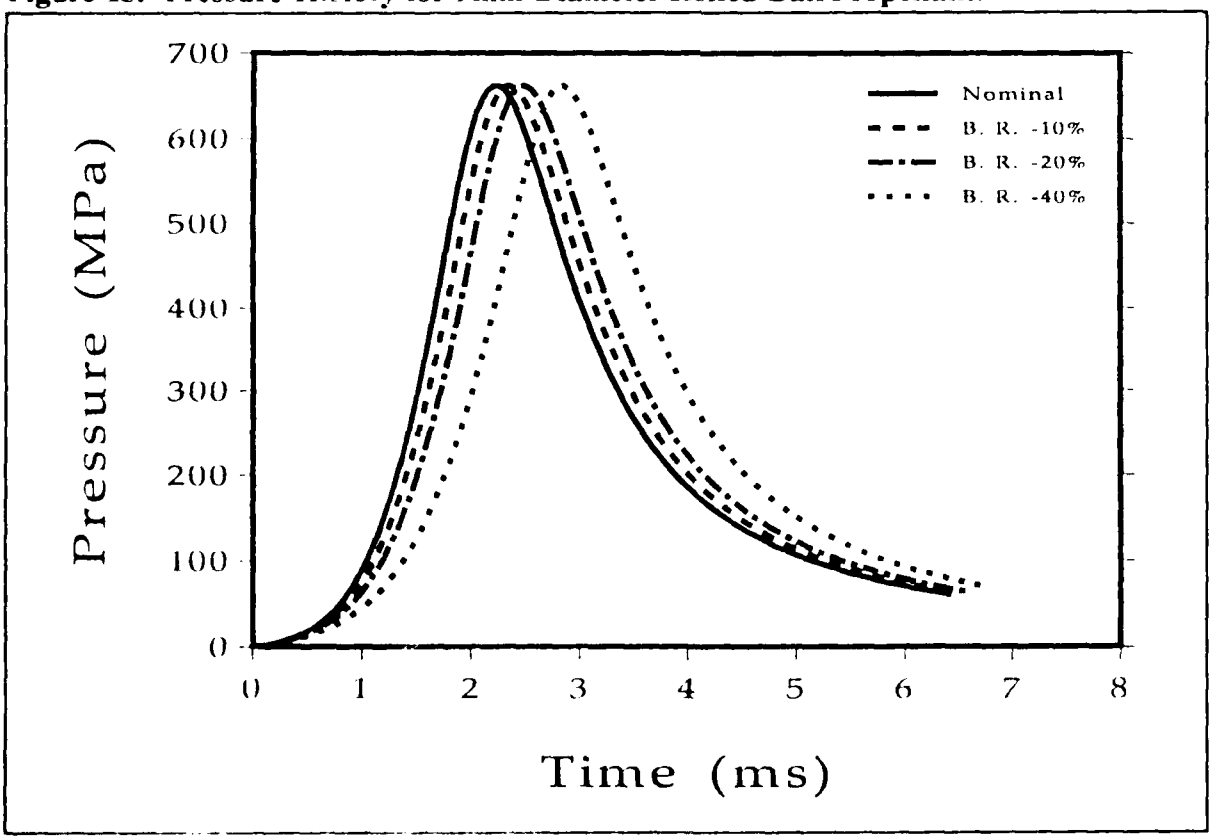

In order to compare deterrent effects to the previous geometry study, one may use the same deterrent layer on the 9-millimeter rolled-ball grain from the geometry optimization study (Table 11, which includes data from Table 7). In terms of charge weight needed to get a particular pressure level, and in terms of temperature sensitivity, the different levels of deterrent now fit neatly between the original non-deterred grain and the single-perf charge. If a greater reduction in burning rate were used, or its profile extended deeper into the grain, the deterred propellant velocities could well extend into the multi-perf range of performance. On the negative side - note also that as performance increases, so does the temperature sensitivity.

The Travel column again shows that the timing of the maximum pressure event can be controlled via deterrents. As the deterrent level increases in the rolled-ball charge, so does this distance. Similar to the trend noted in Figures 6 and 7, exit velocities rise as position of P_{MAX} is moved away from breech face. When the reservoir of high-pressure propellant product gases is larger, base pressures are greater for the remaining projectile travel, resulting in greater accelerations and higher exit velocities.

Table 11. Optimized Geometry and Deterrent Comparisons.

Geometry	Chg Wt (kg)	Ambient P_{MAX} (MPa)	Ambient Vel (m/s)	Hot P_{MAX} (MPa)	Hot Vel (m/s)	Travel (cm)	ΔP (MPa)
Sphere*	6.95	565.4	1383	662.6	1449	28.50	97.2
R-Ball (N-D)†	6.90	555.0	1437	661.5	1497	33.56	106.5
R-Ball (10%)†	7.05	551.6	1444	662.7	1507	35.56	111.1
R-Ball (20%)†	7.15	546.4	1451	662.3	1515	38.28	115.9
R-Ball (40%)†	7.60	532.6	1469	662.5	1543	45.50	129.9
1-Perf ‡	7.95	529.2	1489	661.3	1577	44.05	132.1
7-Perf ‡	8.85	486.8	1518	662.5	1629	75.64	175.7
19-Perf ‡	9.35	460.6	1516	661.8	1644	103.50	201.2

Notes:
* Burned at exit: 6.45 kg Ambient, 6.71 kg Hot
† Major Diameter = 9.0 mm ; Diameter/Thickness ≃ 3.5
‡ Length = 0.5 m ; Perf Diam = 0.762 mm

5. IGNITION DELAY

Recently the Olin Corporation and BRL have tested a compacted form of the rolled Ball Powder® propellant for use in a 120-mm gun system. Deterred propellant grains are lightly coated with a binder material, then pressed into a cylindrical shape with an outer diameter to fit into a combustible case. Cylinder lengths are controlled so that the pressed material can be stacked to form partial or full charges inside the case. A central perforation is used for ignition and flame-spreading purposes as well as providing in-chamber volume for projectile intrusions. Figure 14 is a picture of various examples of the pressed, stackable cylinders. (Photograph provided courtesy of Olin Corporation, Smokeless Powder Division, St. Marks, FL.)

Figure 14. Examples of Compacted-charge Cylinders.

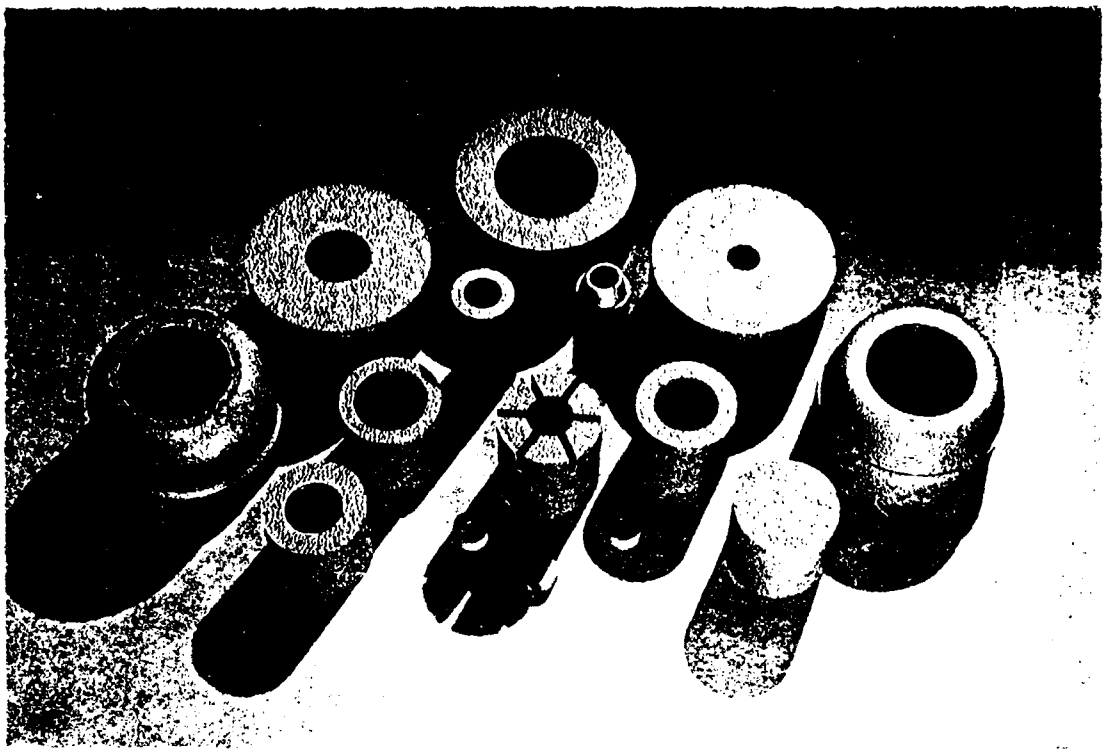

Figure 15. Ignition Delay Function.

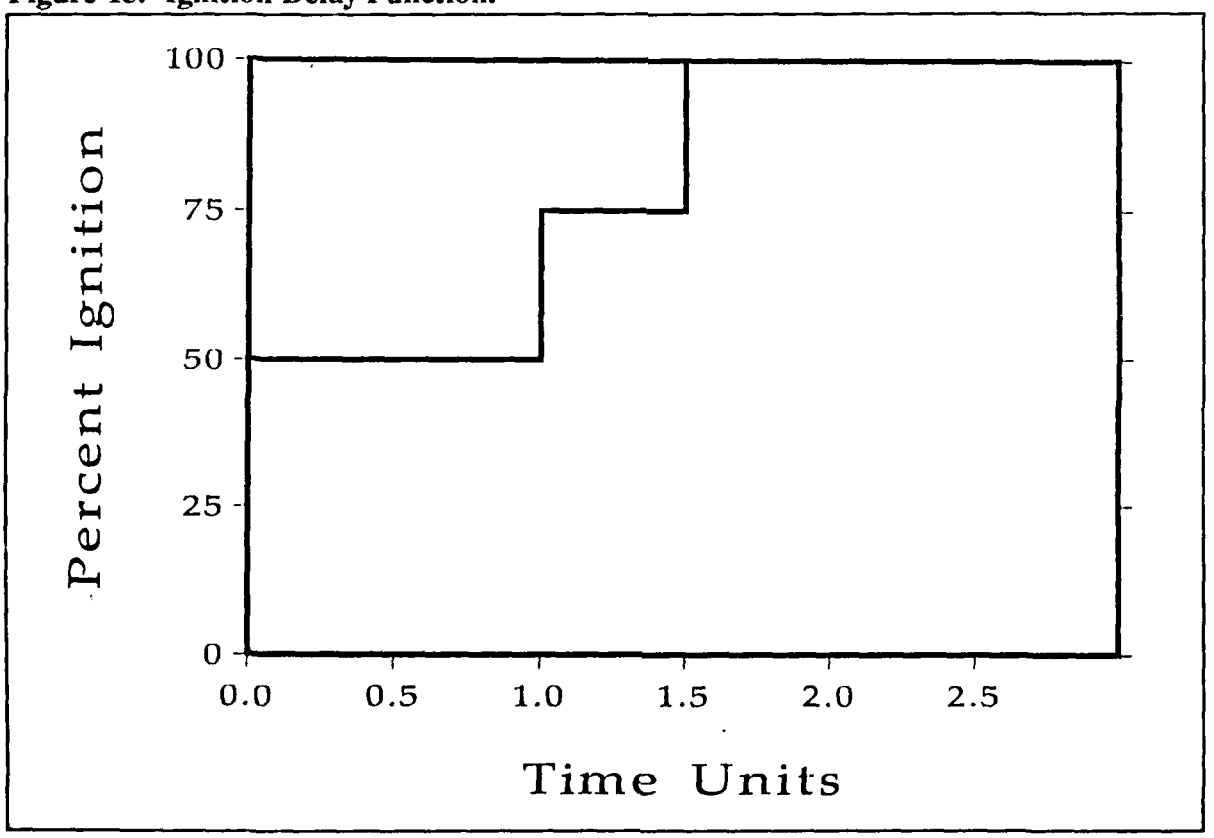

Successful modelling of the compacted charge has been done by Olin with the IBHVG2 program.[4] An ignition-delay feature, where one or more parts of the main charge can be ignited after a user-selectable interval, is the mechanism which seems to give best results.

If real, the ignition delays could be caused by:

1. Small surface cracks in a low percentage of grains, created by the rolling process, which allow flames into the interior high-burning-rate material. When cold, the grains are brittle and tend to fracture from gas pressure within the fissures, exposing more surface area and causing a rapid initial chamber pressurization. At higher pre-ignition temperatures the grains are not as brittle, would not break as rapidly, and would not be as big a factor in the initial chamber pressurization.

2. Binder material exhibiting a temperature-dependent response to the ignition process. In a cold situation the binder would see pressurization as a mechanical shock, causing a rapid deconsolidation of the glued particles. If the binder is less brittle at higher temperatures, the deconsolidation will not be as rapid -- the compacted charge would tend to be "mushier" and would slow the flamespreading process.

Both of these ideas tend to explain the deconsolidation process as a mechanical temperature-dependent phenomenon, where surface availability of individual grains is controlled by physical breakup of the compacted mass. As the temperature decreases, the deconsolidation rate increases, and the net result is faster flamespreading to the individual rolled-ball grains.

Whatever the mechanism, it will be portrayed here as an ignition-delay function, where one-half of the charge will ignite immediately. After one time unit, another one-quarter of the charge will ignite. The remaining propellant will ignite after one-and-one-half time units. This will correspond to a "speed-up" in the flamespreading process. "Time units" will vary from zero to two milliseconds in steps of one-half millisecond of interior ballistic time. The step-function of time-units versus charge ignition is graphed in Figure 15.

Table 12 shows computations for three rolled-ball propellants -- one with no deterred layer, the second with a DT20 layer, and the third with a DT40 layer. These grains use the same major diameter and thickness as found in Table 11, and have not been optimized for best velocity performance. The purpose of this ignition delay study is to look for trends in performance and temperature sensitivity, and the granulation need not be optimized here.

Table 12. Ignition Delay Computations.

Deterrent/ Geometry	Delay (ms)	Chg Wt (kg)	Ambient P_{MAX} (MPa)	Ambient Vel (m/s)	Hot P_{MAX} (MPa)	Hot Vel (m/s)	ΔP (MPa)
R-B(ND)	0.0	6.90	555.0	1437	661.5	1497	106.5
R-B(ND)	0.5	6.916	555.3	1438	661.8	1498	106.5
R-B(ND)	1.0	6.980	556.3	1442	661.7	1502	105.4
R-B(ND)	1.5	7.194	560.4	1455	662.0	1514	101.6
R-B(ND)	2.0	8.002	572.3	1500	661.8	1557	89.5
R-B(DT20)	0.0	7.15	546.4	1451	662.3	1515	115.9
R-B(DT20)	0.5	7.164	546.4	1451	662.1	1515	115.7
R-B(DT20)	1.0	7.220	547.3	1455	662.1	1518	114.8
R-B(DT20)	1.5	7.392	550.5	1465	662.2	1528	111.7
R-B(DT20)	2.0	7.940	558.8	1495	662.3	1556	103.5
R-B(DT40)	0.0	7.60	532.6	1469	662.5	1543	129.9
R-B(DT40)	0.5	7.612	532.1	1469	661.6	1543	129.5
R-B(DT40)	1.0	7.662	532.9	1472	661.6	1545	128.7
R-B(DT40)	1.5	7.806	535.8	1480	662.1	1552	126.3
R-B(DT40)	2.0	8.212	542.0	1501	661.9	1571	119.9
7-Perf	0.0	8.85	486.8	1518	662.5	1629	175.7
7-Perf	0.5	8.870	486.8	1518	662.3	1630	175.5
7-Perf	1.0	8.940	487.0	1521	662.4	1632	175.4
7-Perf	1.5	9.138	488.0	1529	662.0	1638	174.0
7-Perf	2.0	9.748	491.0	1549	661.8	1656	170.8
19-Perf	0.0	9.35	460.6	1516	661.8	1644	201.2
19-Perf	0.5	9.372	460.3	1517	661.7	1645	201.4
19-Perf	1.0	9.445	460.6	1519	662.1	1646	201.5
19-Perf	1.5	9.646	461.6	1526	662.1	1651	200.5
19-Perf	2.0	10.272	465.1	1545	662.0	1668	196.9

At zero time delay, the maximum pressures and exit velocities are computed to be the same as when the charge was treated as a single unit. Then the ignition delays are inserted for the two smaller charge sections. For the computation where ignition delay is 1.5 millisecond, the computation used one-and-one-half millisecond delay before igniting the first quarter-charge unit, then another half time-unit (for a total of two-and-one-quarter milliseconds) before igniting the remaining quarter-charge.

Charge weights have been adjusted so that all hot maximum pressures are close to 662 MPa. The difference between these hot maximum breech pressures and the corresponding ambient maximum breech pressures will give us a measure of the changes in temperature sensitivity. Trends are:

1. As ignition delay increases, ΔP falls -- suggesting a negative

temperature sensitivity correlation.

2. For each grain type, velocities rise as ignition delay times increase.

A comparison of the non-deterred rolled-ball grains versus 7-Perf and 19-Perf grains can also be seen in Table 12. Again, the dimensions of all geometries were taken directly from the previous two optimizations. Trends are similar in that ignition delay has a negative temperature sensitivity function, and velocities increase as the delay moves position of maximum breech pressure event later in the ballistic cycle. Still evident for the progressive grains are the high differentials between ambient and hot maximum breech pressures. The perforated grains show less of a change in temperature sensitivity than do the rolled-ball charges over the range of time delays.

Figure 16 is a graph of the five breech pressure profiles versus ballistic time for the 662 MPa computations ("hot" charges) with 2.0 ms ignition delays. The breaks at 2.0 and 3.0 milliseconds are the ignition points of the two quarter-charges. It is evident that increases in deterrent strength have moved ballistic time of pressure maximums dramatically in the direction of the multi-perf cases.

Figure 16. Pressure Histories from 2.0-ms Ignition Delay Calculations.

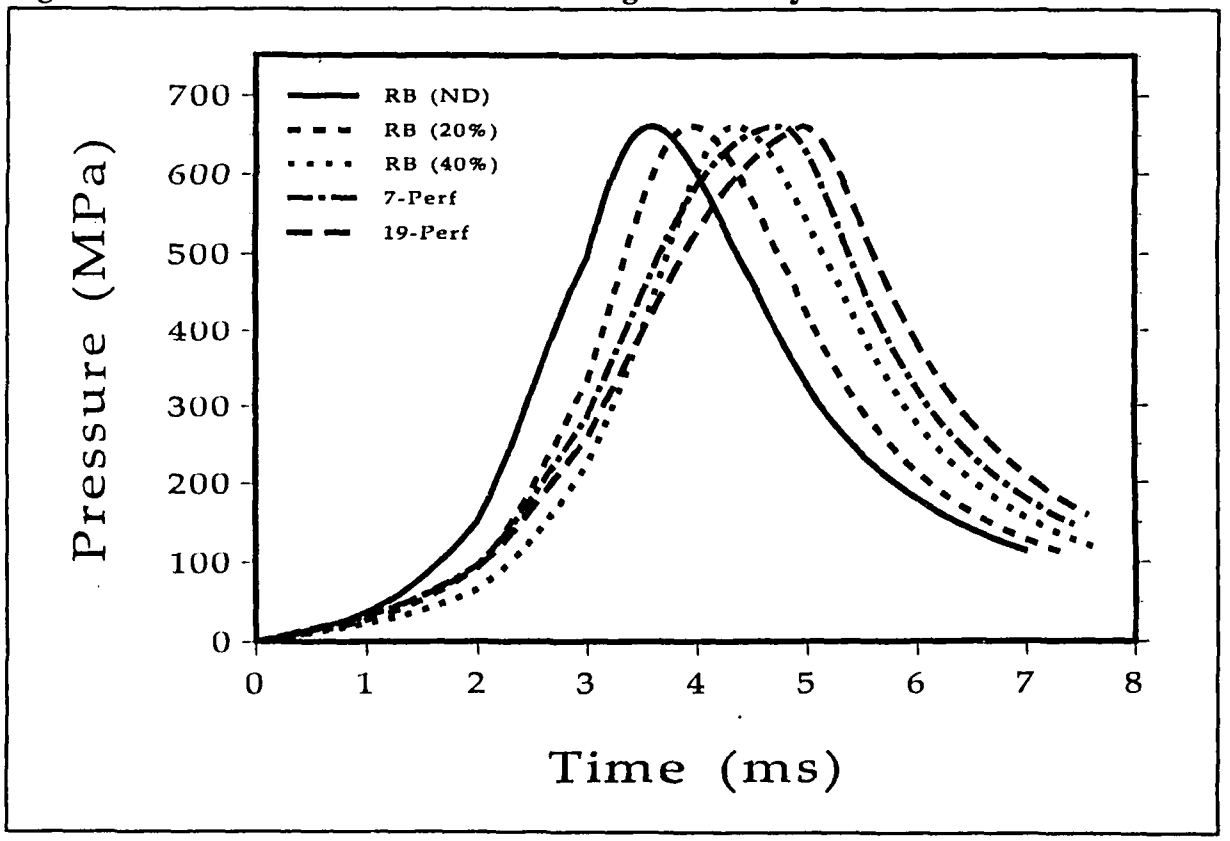

A self-limiting factor for ignition delays is that as the delay becomes longer, the charge may not have time to burn completely. A major difference between the five cases is that the last quarter-charge of the perforated grains and the ND rolled-ball grain

did not burn out completely at the time of projectile exit, while the DT20 and DT40 grains seemed to burn out well before exit. The data in Table 13 are from the computations at the maximum time delay (2.0 milliseconds). Early burnout of the deterred rolled-ball cases may suggest that the optimum grain could be thicker and might result in even higher velocities.

Table 13. Mass Fractions at Projectile Exit.

Grain		Status
R-Ball (ND)	-	99.3% Burned at Projectile Exit
R-Ball (20%)	-	Burned Out at 3.866 m Travel
R-Ball (40%)	-	Burned Out at 3.501 m Travel
7-Perf	-	98.8% Burned at Projectile Exit
19-Perf	-	97.6% Burned at Projectile Exit

At the present time, not enough is known about deconsolidation rates to make a truly optimum-design compacted artillery charge. Multi-perf propellants may not lend themselves to the compaction process as well as do rolled-ball grains, because of deformation and closure of internal gas flow channels (perforations). Relationships between binder chemistry, the manufacturing process, mechanical stress in the compacted charge, and many other variables, are yet to be fully researched. But the ability to control propellant flamespreading would be an important step in advancing charge design.

6. SUMMARY

From this limited theoretical study of grain geometry, deterrent effects, and ignition strategies, several trends have become evident:

1. The three temperature sensitivity factors studied here all derive their performance increases from controlling the timing of the maximum pressure event.

   Geometry effects control burning surface availability for the individual grains.

   Deterrent layering controls energy release rate as a function of burned depth.

   Ignition delays control the burning surface area in terms of the number of propellant grains ignited at a particular ballistic time.

2. Regressive geometries are inherently less temperature-sensitive.

3. Deterred layers increase temperature sensitivity, but may allow more propellant in the chamber for a given maximum breech pressure - resulting in more energy transfer to a projectile and better exit velocity performance.

4. Compaction-induced ignition delays reduce temperature sensitivity and may also increase system performance.

The combination of regressive geometry, deterrent layering, and ignition delays can increase the performance of the rolled-ball propellants so that they may challenge velocity levels of the multi-perforated charges, yet keep temperature sensitivity levels low enough to be very attractive for large-caliber gun systems.

THIS PAGE INTENTIONALLY LEFT BLANK.

7. REFERENCES

[1] Anderson, R. D., and Fickie, K. D., "IBHVG2 -- A User's Guide," BRL-TR-2829, Ballistic Research Laboratory, Aberdeen Proving Ground, MD, July 1987.

[2] Oberle, W. F., Ballistic Research Laboratory, Aberdeen Proving Ground, MD, Private Communication, July 1989.

[3] Freedman, E., "BLAKE - A Thermodynamics Code Based on TIGER: Users' Guide and Manual," ARBRL-TR-02411, Ballistic Research Laboratory, Aberdeen Proving Ground, July 1982.

[4] Gonzalez, A. F., Olin Corporation, St. Marks, FL, Private Communication, July 1989.

THIS PAGE INTENTIONALLY LEFT BLANK.

APPENDIX A:

Sample IBHVG2 Input for Data in Figure 1

THIS PAGE INTENTIONALLY LEFT BLANK.

```
$GUN
      NAME = 'GERMAN 120MM GUN'      TRAV = 4.7498      TWST = 99
      GRVE = 0.11999          LAND = 0.11999    G/L  = 1.
      CHAM=0.00920953
$PROJ
      NAME = 'APFSDS'         PRWT = 9.52544
$RESI
      NPTS = 4                AIR  = 1
      TRAV =       0,      0.02032,       0.0762,     4.7498
      PRES =   0.6895,      17.237,       0.3447,     0.3447
$HEAT
      HL=1                    TSHL = 0.0001143
$INFO
      RUN='TEMPERATURE SENSITIVITY - GEOMETRY - 1PF AMB'
      DELT = 5E-5             DELP = 5E-5
      GRAD = 2                POPT = 1,1,1,0,0  SOPT = 0
      EPS  = 0.002            CONP = 0
$RECO
      NAME = 'NONE'           RECO = 0          ROWT = 0
$PRIM
      NAME = 'BLK PWD'        CHWT = 0.0009979
      GAMA = 1.25             FORC = 295918.
      COV  = 0.0010838        TEMP = 2000
$PROP
      NAME = 'BLK PWD'        CHWT = 0.09988    GRAN = 'CORD'
      RHO  = 1660.794         GAMA = 1.219      FORC = 295918.
      COV  = 0.0010838        TEMP = 2000       EROS = 0.00000
      ALPH = 0                BETA = 1.27       IGNC = 0
      LEN  = 0.0050292        DIAM = 0.0024892
$PROP
      NAME = '1PF AMBIENT'     CHWT = 8.5       GRAN = '1PF'
      RHO  = 1600.00          GAMA = 1.2247     FORC = 1143219.5
      COV  = 0.000938         TEMP = 3558       EROS = 0.0000000
      LEN  = 0.5              PD   = 0.000762   WEB  = 0.0029358
      NTBL = 4  PR4L = 68.95,  137.89, 206.84, 275.79
                BR4L = 0.0763, 0.1383, 0.2034, 0.2626
$END
$SAVE
$INFO
      RUN='TEMPERATURE SENSITIVITY - GEOMETRY - 1PF HOT'
$PROP
$PROP
      NAME = '1PF HOT'
      NTBL = 4  PR4L = 68.95,  137.89, 206.84, 275.79
                BR4L = 0.0811, 0.1470, 0.2110, 0.2832
$END
```

THIS PAGE INTENTIONALLY LEFT BLANK.

APPENDIX B:

Sample IBHVG2 Input for Data in Figures 2 and 3

THIS PAGE INTENTIONALLY LEFT BLANK.

```
$GUN
      NAME = 'GERMAN 120MM GUN'      TRAV = 4.7498      TWST = 99
      GRVE = 0.11999          LAND = 0.11999    G/L  = 1.
      CHAM=0.00920953
$PROJ
      NAME = 'APFSDS'         PRWT = 9.52544
$RESI
      NPTS = 4                AIR  = 1
      TRAV =       0,      0.02032,       0.0762,     4.7498
      PRES =  0.6895,      17.237,       0.3447,     0.3447
$HEAT
      HL=1                    TSHL = 0.0001143

$INFO
      RUN='TEMPERATURE SENSITIVITY - GEOMETRY - BALL AMB'
      DELT = 5E-5             DELP = 5E-5
      GRAD = 2                POPT = 1,1,1,0,0  SOPT = 0
      EPS  = 0.002            CONP = 0

$RECO
      NAME = 'NONE'           RECO = 0          ROWT = 0
$PRIM
      NAME = 'BLK PWD'        CHWT = 0.0009979
      GAMA = 1.25             FORC = 295918.
      COV  = 0.0010838        TEMP = 2000
$PROP
      NAME = 'BLK PWD'        CHWT = 0.09988    GRAN = 'CORD'
      RHO  = 1660.794         GAMA = 1.219      FORC = 295918.
      COV  = 0.0010838        TEMP = 2000       EROS = 0.00000
      ALPH = 0                BETA = 1.27       IGNC = 0
      LEN  = 0.0050292        DIAM = 0.0024892
$PROP
      NAME = 'BALL AMBIENT'     CHWT = 8.5      GRAN = 'BALL'
      RHO  = 1600.00          GAMA = 1.2247     FORC = 1143219.5
      COV  = 0.000938         TEMP = 3558       EROS = 0.0000000
      DIAM = .007855
      NTBL = 4  PR4L = 68.95,  137.89, 206.84, 275.79
                BR4L = 0.0763, 0.1383, 0.2034, 0.2626
$END
$SAVE
$INFO
      RUN='TEMPERATURE SENSITIVITY - GEOMETRY - BALL HOT'
$PROP
$PROP
      NTBL = 4  PR4L = 68.95,  137.89, 206.84, 275.79
                BR4L = 0.0811, 0.1470, 0.2110, 0.2832
```

```
$END
$SAVE
$INFO
      RUN='TEMPERATURE SENSITIVITY - GEOMETRY - 1PF AMB'
$PROP
$PROP
      NAME = '1PF AMBIENT'     GRAN = '1PF'
      LEN  = 0.5            PD   = 0.000762   WEB  = 0.0029358
      NTBL = 4  PR4L = 68.95,  137.89, 206.84, 275.79
                BR4L = 0.0763, 0.1383, 0.2034, 0.2626
$END
$SAVE
$INFO
      RUN='TEMPERATURE SENSITIVITY - GEOMETRY - 1PF HOT'
$PROP
$PROP
      NTBL = 4  PR4L = 68.95,  137.89, 206.84, 275.79
                BR4L = 0.0811, 0.1470, 0.2110, 0.2832
$END
$SAVE
$INFO
      RUN='TEMPERATURE SENSITIVITY - GEOMETRY - 19PF AMB'
$PROP
$PROP
      NAME = '19PF AMBIENT'    GRAN = '19PF'
      LEN  = 0.5            PD   = 0.000762   WEB  = 0.00195396
      NTBL = 4  PR4L = 68.95,  137.89, 206.84, 275.79
                BR4L = 0.0763, 0.1383, 0.2034, 0.2626
$END
$SAVE
$INFO
      RUN='TEMPERATURE SENSITIVITY - GEOMETRY - 19PF HOT'
$PROP
$PROP
      NTBL = 4  PR4L = 68.95,  137.89, 206.84, 275.79
                BR4L = 0.0811, 0.1470, 0.2110, 0.2832
$END
```

APPENDIX C:

Sample IBHVG2 Input for DT20 Data in Table 11

THIS PAGE INTENTIONALLY LEFT BLANK.

```
$GUN
      NAME = 'GERMAN 120MM GUN'      TRAV = 4.7498      TWST = 999
      GRVE = 0.11999          LAND = 0.11999     G/L  = 1.
      CHAM=0.00920953
$PROJ
      NAME = 'APFSDS'         PRWT = 9.52544
$RESI
      NPTS = 4                AIR  = 1
      TRAV =       0,      0.02032,       0.0762,     4.7498
      PRES =   0.6895,      17.237,        0.3447,     0.3447
$HEAT
      HL=1                    TSHL = 0.0001143
$INFO
      RUN='DETERRED ROLLED BALL - AMB .8BR - AMB PMAX=544.68'
      DELT = 5E-5             DELP = 5E-5
      GRAD = 2                POPT = 1,0,1,0,0   SOPT = 0
      EPS  = 0.002            CONP = 0
$RECO
      NAME = 'NONE'           RECO = 0           RCWT = 0
$PRIM
      NAME = 'BLK PWD'        CHWT = 0.0009979
      GAMA = 1.25             FORC = 295918.
      COV  = 0.0010838        TEMP = 2000
$PROP
      NAME = 'BLK PWD'        CHWT = 0.09988     GRAN = 'CORD'
      RHO  = 1660.794         GAMA = 1.219       FORC = 295918.
      COV  = 0.0010838        TEMP = 2000        EROS = 0.00000
      ALPH = 0                BETA = 1.27        IGNC = 0
      LEN  = 0.0050292        DIAM = 0.0024892
$COMMENT    USE OPTIMIZED DIMENSIONS TO CHECK HOT FOR PRESSURE LIMIT
$PROP
      NAME = 'ROLLED BALL'      CHWT = 7.20      GRAN = 'PAN'
      RHO  = 1600.00          GAMA = 1.2247      FORC = 1143219.5
      COV  = 0.000938         TEMP = 3558        EROS = 0.0000000
      DIAM = 0.0090           THCK=.0024429

      NTBL = 4  PR4L = 68.95,  137.89, 206.84, 275.79
                BR4L = 0.0763, 0.1383, 0.2034, 0.2626

      DEPL=0,0,.000352425   $ .8 B.R.

               PR3L = 68.95,   137.89,  206.84,   275.79
               BR3L = 0.06104, 0.11064, 0.16272,  0.21008

$COMMENT    INITIAL CALCULATIONS TO FIND OPTIMIZED DIMENSIONS
   $PMAX
```

```
      VARY='THCK' NTH=2 TRY1=0.0024 TRY2=0.0025 PMAX=548.13 EPS=.01
   $PARA
      VARY='CHWT' DECK='PROP' NTH=2 FROM=6.5 BY=0.05 TO=7.5
   $END
   $SAVE
   $INFO
      RUN='OPTIM AT 551.58 MPA'
   $PMAX
      PMAX=551.58
   $END
   $SAVE
   $INFO
      RUN='OPTIM AT 555.03 MPA'
   $PMAX
      PMAX=555.03
$END

$COMMENT   USE OPTIMIZED DIMENSIONS TO CHECK FOR HOT PRESSURE LIMIT
$SAVE
$INFO
      RUN='DETERRED ROLLED BALL - HOT .8BR - AMB PMAX=544.68'
$PROP
$PROP
      NTBL = 4  PR4L = 68.95,  137.89, 206.84, 275.79
                BR4L = 0.0811, 0.1470, 0.2110, 0.2832

      DEPL=0,0,.000352425   $ .8 B.R.

               PR3L = 68.95,   137.89,  206.84,   275.79
               BR3L = 0.06488, 0.1176, 0.1688, 0.22656
$END
$SAVE
$INFO
      RUN='DETERRED ROLLED BALL - AMB .8BR - AMB PMAX=546.41'
$PROP
$PROP
      CHWT = 7.15      THCK = 0.0023933
      NTBL = 4  PR4L = 68.95,  137.89, 206.84, 275.79
                BR4L = 0.0763, 0.1383, 0.2034, 0.2626

      DEPL=0,0,.000352425   $ .8 B.R.

               PR3L = 68.95,   137.89,  206.84,   275.79
               BR3L = 0.06104, 0.11064, 0.16272,  0.21008
$END
$SAVE
```

```
$INFO
      RUN='DETERRED ROLLED BALL - HOT .8BR - AMB PMAX=546.41'
$PROP
$PROP
      NTBL = 4  PR4L = 68.95,  137.89, 206.84, 275.79
                BR4L = 0.0811, 0.1470, 0.2110, 0.2832

      DEPL=0,0,.000352425   $ .8 B.R.

                PR3L = 68.95,   137.89,  206.84,   275.79
                BR3L = 0.06488, 0.1176, 0.1688, 0.22656
$END
$SAVE
$INFO
      RUN='DETERRED ROLLED BALL - HOT .8BR - AMB PMAX=548.13'
$PROP
$PROP
      CHWT = 7.20      THCK = 0.0024297
      NTBL = 4  PR4L = 68.95,  137.89, 206.84, 275.79
                BR4L = 0.0763, 0.1383, 0.2034, 0.2626

      DEPL=0,0,.000352425   $ .8 B.R.

                PR3L = 68.95,   137.89,  206.84,   275.79
                BR3L = 0.06104, 0.11064, 0.16272,  0.21008
$END
$SAVE
$INFO
      RUN='DETERRED ROLLED BALL - HOT .8BR - AMB PMAX=548.13'
$PROP
$PROP
      NTBL = 4  PR4L = 68.95,  137.89, 206.84, 275.79
                BR4L = 0.0811, 0.1470, 0.2110, 0.2832

      DEPL=0,0,.000352425   $ .8 B.R.

                PR3L = 68.95,   137.89,  206.84,   275.79
                BR3L = 0.06488, 0.1176, 0.1688, 0.22656
$END
```

THIS PAGE INTENTIONALLY LEFT BLANK.

APPENDIX D:

Sample IBHVG2 Input for DT40 Data in Figure 16

THIS PAGE INTENTIONALLY LEFT BLANK.

```
$GUN
      NAME = 'GERMAN 120MM GUN'      TRAV = 4.7498      TWST = 999
      GRVE = 0.11999          LAND = 0.11999     G/L  = 1.
      CHAM=0.00920953
$PROJ
      NAME = 'APFSDS'         PRWT = 9.52544
$RESI
      NPTS = 4                AIR  = 1
      TRAV =       0,      0.02032,       0.0762,     4.7498
      PRES =   0.6895,      17.237,       0.3447,     0.3447
$HEAT
      HL=1                    TSHL = 0.0001143
$INFO
      RUN='ROLLED BALL AMB - .6 BR - DELAY = 2.00 MS'
      DELT = 5E-5             DELP = 5E-5
      GRAD = 2                POPT = 1,1,1,0,2  SOPT = 0
      EPS  = 0.002            CONP = 0
      $ DET ROLLED-BALL, .6 X BURN RATE
$RECO
      NAME = 'NONE'           RECO = 0          ROWT = 0
$PRIM
      NAME = 'BLK PWD'        CHWT = 0.0009979
      GAMA = 1.25             FORC = 295918.
      COV  = 0.0010838        TEMP = 2000
$PROP
      NAME = 'BLK PWD'        CHWT = 0.09988    GRAN = 'CORD'
      RHO  = 1660.794         GAMA = 1.219      FORC = 295918.
      COV  = 0.0010838        TEMP = 2000       EROS = 0.00000
      ALPH = 0                BETA = 1.27       IGNC = 0
      LEN  = 0.0050292        DIAM = 0.0024892
$PROP
      NAME = 'R-BALL DET 40 - AMB'    CHWT = 4.106   GRAN = 'PAN'
      RHO  = 1600.00          GAMA = 1.2247     FORC = 1143219.5
      COV  = 0.000938         TEMP = 3558       EROS = 0.0000000
      DIAM = 0.0090           THCK=.0023750
      NTBL = 4  PR4L = 68.95,  137.89, 206.84, 275.79
                BR4L = 0.0763, 0.1383, 0.2034, 0.2626
      DEPL=0,0,.000352425   $ .6 B.R.
               PR3L = 68.95,   137.89,  206.84,   275.79
               BR3L = 0.04578, 0.08298, 0.120204,  0.15756
$PROP
      NAME = 'R-BALL DET 40 - AMB'    CHWT = 2.053   GRAN = 'PAN'
      RHO  = 1600.00          GAMA = 1.2247     FORC = 1143219.5
      COV  = 0.000938         TEMP = 3558       EROS = 0.0000000
      DIAM = 0.0090           THCK=.0023750
      IGNC = 1                THRC = 0.00200   $ IGNITE AT 2.0 MS
```

```
     NTBL = 4  PR4L = 68.95,  137.89, 206.84, 275.79
               BR4L = 0.0763, 0.1383, 0.2034, 0.2626
     DEPL=0,0,.000352425   $ .6 B.R.
              PR3L = 68.95,    137.89,  206.84,   275.79
              BR3L = 0.04578, 0.08298, 0.120204,  0.15756
$PROP
     NAME = 'R-BALL DET 40 - AMB'   CHWT = 2.053   GRAN = 'PAN'
     RHO  = 1600.00        GAMA = 1.2247     FORC = 1143219.5
     COV  = 0.000938       TEMP = 3558       EROS = 0.0000000
     DIAM = 0.0090         THCK=.0023750
     IGNC = 1              THRC = 0.00300   $ IGNITE AT 3.0 MS
     NTBL = 4  PR4L = 68.95,  137.89, 206.84, 275.79
               BR4L = 0.0763, 0.1383, 0.2034, 0.2626
     DEPL=0,0,.000352425   $ .6 B.R.
              PR3L = 68.95,    137.89,  206.84,   275.79
              BR3L = 0.04578, 0.08298, 0.120204,  0.15756
$END
$SAVE
$INFO
     RUN='ROLLED BALL HOT - .6 BR - DELAY = 2.00 MS'
$PROP
$PROP
     NTBL = 4  PR4L = 68.95,  137.89, 206.84, 275.79
               BR4L = 0.0811, 0.1470, 0.2110, 0.2832
     DEPL=0,0,.000352425   $ .6 B.R.
              PR3L = 68.95,    137.89,  206.84,   275.79
              BR3L = 0.04866, 0.0882, 0.1266, 0.16992
$PROP
     NTBL = 4  PR4L = 68.95,  137.89, 206.84, 275.79
               BR4L = 0.0811, 0.1470, 0.2110, 0.2832
     DEPL=0,0,.000352425   $ .6 B.R.
              PR3L = 68.95,    137.89,  206.84,   275.79
              BR3L = 0.04866, 0.0882, 0.1266, 0.16992
$PROP
     NTBL = 4  PR4L = 68.95,  137.89, 206.84, 275.79
               BR4L = 0.0811, 0.1470, 0.2110, 0.2832
     DEPL=0,0,.000352425   $ .6 B.R.
              PR3L = 68.95,    137.89,  206.84,   275.79
              BR3L = 0.04866, 0.0882, 0.1266, 0.16992
$END
```

No of Copies | Organization

2 Administrator
Defense Technical Info Center
ATTN: DTIC-DDA
Cameron Station
Alexandria, VA 22304-6145

1 HQDA (SARD-TR)
WASH DC 20310-0001

1 Commander
US Army Materiel Command
ATTN: AMCDRA-ST
5001 Eisenhower Avenue
Alexandria, VA 22333-0001

1 Commander
US Army Laboratory Command
ATTN: AMSLC-DL
Adelphi, MD 20783-1145

2 Commander
US Army, ARDEC
ATTN: SMCAR-IMI-I
Picatinny Arsenal, NJ 07806-5000

2 Commander
US Army, ARDEC
ATTN: SMCAR-TDC
Picatinny Arsenal, NJ 07806-5000

1 Director
Benet Weapons Laboratory
US Army, ARDEC
ATTN: SMCAR-CCB-TL
Watervliet, NY 12189-4050

1 Commander
US Army Armament, Munitions
and Chemical Command
ATTN: SMCAR-ESP-L
Rock Island, IL 61299-5000

1 Director
US Army Aviation Research
and Technology Activity
ATTN: SAVRT-R (Library)
M/S 219-3
Ames Research Center
Moffett Field, CA 94035-1000

No of Copies | Organization

1 Commander
US Army Missile Command
ATTN: AMSMI-RD-CS-R (DOC)
Redstone Arsenal, AL 35898-5010

1 Commander
US Army Tank-Automotive Command
ATTN: AMSTA-TSL (Technical Library)
Warren, MI 48397-5000

1 Director
US Army TRADOC Analysis Command
ATTN: ATRC-WSR
White Sands Missile Range, NM 88002-5502

(Class. only) 1 Commandant
US Army Infantry School
ATTN: ATSH-CD (Security Mgr.)
Fort Benning, GA 31905-5660

(Unclass. only) 1 Commandant
US Army Infantry School
ATTN: ATSH-CD-CSO-OR
Fort Benning, GA 31905-5660

1 Air Force Armament Laboratory
ATTN: AFATL/DLODL
Eglin AFB, FL 32542-5000

Aberdeen Proving Ground

2 Dir, USAMSAA
ATTN: AMXSY-D
AMXSY-MP, H. Cohen

1 Cdr, USATECOM
ATTN: AMSTE-TD

3 Cdr, CRDEC, AMCCOM
ATTN: SMCCR-RSP-A
SMCCR-MU
SMCCR-MSI

1 Dir, VLAMO
ATTN: AMSLC-VL-D

No. of Copies Organization

1 Commander
USA Concepts Analysis Agency
ATTN: D. Hardison
8120 Woodmont Avenue
Bethesda, MD 20014-2797

1 C.I.A.
01R/DB/Standard
Washington, DC 20505

1 US Army Ballistic Missile
Defense Systems Command
Advanced Technology Center
P.O. Box 1500
Huntsville, AL 35807-3801

1 Chairman
DoD Explosives Safety Board
Room 856-C
Hoffman Bldg. 1
2461 Eisenhower Avenue
Alexandria, VA 22331-0600

1 Commander
US Army Materiel Command
ATTN: AMCPM-GCM-WF
5001 Eisenhower Avenue
Alexandria, VA 22333-5001

1 Commander
US Army Materiel Command
ATTN: AMCDE-DW
5001 Eisenhower Avenue
Alexandria, VA 22333-5001

3 Project Manager
Autonomous Precision-Guided
Munition (APGM)
US Army, ARDEC
ATTN: AMCPM-CW
AMCPM-CWW
AMCPM-CWA-S, R. DeKleine
Picatinny Arsenal, NJ 07806-5000

2 Project Manager
Production Base Modernization Agency
ATTN: AMSMC-PBM, A. Siklosi
AMSMC-PBM-E, L. Laibson
Picatinny Arsenal, NJ 07806-5000

No. of Copies Organization

3 PEO-Armaments
Project Manger
Tank Main Armament Systems
ATTN: AMCPM-TMA, K. Russell
AMCPM-TMA-105
AMCPM-TMA-120, C. Roller
Picatinny Arsenal, NJ 07806-5000

1 Commander
US Army, ARDEC
ATTN: SMCAR-AEE
Picatinny Arsenal, NJ 07806-5000

13 Commander
US Army, ARDEC
ATTN: SMCAR-AEE-B,
A. Beardell
B. Brodman
P. Bostonian
R. Cirincione
D. Downs
S. Einstein
A. Grabowsky
P. Hui
J. O'Reilly
N. Ross
S. Westley
S. Bernstein
J. Rutkowski
Picatinny Arsenal, NJ 07806-5000

2 Commander
US Army, ARDEC
ATTN: SMCAR-AES,
S. Kaplowitz
D. Spring
Picatinny Arsenal, NJ 07806-5000

2 Commander
US Army, ARDEC
ATTN: SMCAR-HFM, E. Barrieres
SMCAR-CCH-V, C. Mandala
Picatinny Arsenal, NJ 07806-5000

1 Commander
US Army, ARDEC
ATTN: SMCAR-FSA-T, M. Salsbury
Picatinny Arsenal, NJ 07806-5000

No. of Copies	Organization
1	Commander, USACECOM R&D Technical Library ATTN: ASQNC-ELC-I-T, Myer Center Fort Monmouth, NJ 07703-5301
1	Commander US Army Harry Diamond Laboratories ATTN: SLCHD-TA-L 2800 Powder Mill Rd Adelphi, MD 20783-1145
1	Commandant US Army Aviation School ATTN: Aviation Agency Fort Rucker, AL 36360
1	Project Manager US Army Tank-Automotive Command Improved TOW Vehicle ATTN: AMCPM-ITV Warren, MI 48397-5000
2	Program Manager US Army Tank-Automotive Command ATTN: SFAE-ASM-SS-T, T. Dean Warren, MI 48092-2498
1	Project Manager US Army Tank-Automotive Command Fighting Vehicle Systems ATTN: AMCPM-BFVS Warren, MI 48092-2498
1	President US Army Armor and Engineer Board ATTN: ATZK-AD-S Fort Knox, KY 40121-5200
1	Project Manager US Army Tank-Automotive Command M-60 Tank Development ATTN: AMCPM-ABMS Warren, MI 48092-2498
1	Director HQ, TRAC RPD ATTN: ATCD-MA Fort Monroe, VA 23651-5143

No. of Copies	Organization
2	Director US Army Materials Technology Laboratory ATTN: SLCMT-ATL Watertown, MA 02172-0001
1	Commander US Army Research Office ATTN: Technical Library P. O. Box 12211 Research Triangle Park, NC 27709-2211
1	Commander US Army Belvoir Research and Development Center ATTN: STRBE-WC Fort Belvoir, VA 22060-5006
1	Director US Army TRAC-Ft Lee ATTN: ATRC-L, Mr. Cameron Fort Lee, VA 23801-6140
1	Commandant US Army Command and General Staff College Fort Leavenworth, KS 66027
1	Commandant US Army Special Warfare School ATTN: Rev and Tng Lit Div Fort Bragg, NC 28307
3	Commander Radford Army Ammunition Plant ATTN: SMCAR-QA/HI LIB Radford, VA 24141-0298
1	Commander US Army Foreign Science and Technology Center ATTN: AMXST-MC-3 220 Seventh Street, NE Charlottesville, VA 22901-5396

No. of Copies | Organization

2 Commander
Naval Sea Systems Command
ATTN: SEA 62R
SEA 64
Washington, DC 20362-5101

1 Commander
Naval Air Systems Command
ATTN: AIR-954-Technical Library
Washington, DC 20360

1 Assistant Secretary of the Navy
(R, E, and S)
ATTN: R. Reichenbach
Room 5E787
Pentagon Bldg
Washington, DC 20375

1 Naval Research Laboratory
Technical Library
Washington, DC 20375

1 Commandant
US Army Command and General
Staff College
Fort Leavenworth, KS 66027

2 Commandant
US Army Field Artillery Center
and School
ATTN: ATSF-CO-MW, E. Dublisky (2 cys)
Ft. Sill, OK 73503-5600

1 Office of Naval Research
ATTN: Code 473, R. S. Miller
800 N. Quincy Street
Arlington, VA 22217-9999

3 Commandant
US Army Armor School
ATTN: ATZK-CD-MS, M. Falkovitch
Armor Agency
Fort Knox, KY 40121-5215

2 Commander
US Naval Surface Warfare Center
ATTN: J. P. Consaga
C. Gotzmer
Indian Head, MD 20640-5000

No. of Copies | Organization

4 Commander
Naval Surface Warfare Center
ATTN: Code 240, S. Jacobs
Code 730
Code R-13,
K. Kim
R. Bernecker
Silver Spring, MD 20903-5000

2 Commanding Officer
Naval Underwater Systems Center
ATTN: Code 5B331, R. S. Lazar
Technical Library
Newport, RI 02840

5 Commander
Naval Surface Warfare Center
ATTN: Code G33,
J. L. East
W. Burrell
J. Johndrow
Code G23, D. McClure
Code DX-21, Technical Library
Dahlgren, VA 22448-5000

3 Commander
Naval Weapons Center
ATTN: Code 388, C. F. Price
Code 3895, T. Parr
Information Science Division
China Lake, CA 93555-6001

1 OSD/SDIO/IST
ATTN: Dr. Len Caveny
Pentagon
Washington, DC 20332-7100

3 Commander
Naval Ordnance Station
ATTN: T. C. Smith
D. Brooks
Technical Library
Indian Head, MD 20640-5000

1 AL/TSTL (Technical Library)
ATTN: J. Lamb
Edwards AFB, CA 93523-5000

No. of Copies	Organization
1	AFATL/DLYV Eglin AFB, FL 32542-5000
1	AFATL/DLXP Eglin AFB, FL 32542-5000
1	AFATL/DLJE Eglin AFB, FL 32542-5000
1	NASA/Lyndon B. Johnson Space Center ATTN: NHS-22 Library Section Houston, TX 77054
1	AFELM, The Rand Corporation ATTN: Library D 1700 Main Street Santa Monica, CA 90401-3297
3	AAI Corporation ATTN: J. Herbert J. Frankle D. Cleveland P. O. Box 126 Hunt Valley, MD 21030-0126
2	Aerojet Solid Propulsion Company ATTN: P. Micheli L. Torreyson Sarcramento, CA 96813
1	Atlantic Research Corporation ATTN: M. King 5390 Cherokee Avenue Alexandria, VA 22312-2302
3	AL/LSCF ATTN: J. Levine L. Quinn T. Edwards Edwards AFB, CA 93523-5000
1	AVCO Everett Research Laboratory ATTN: D. Stickler 2385 Revere Beach Parkway Everett, MA 02149-5936

No. of Copies	Organization
2	Calspan Corporation ATTN: C. Murphy P. O. Box 400 Buffalo, NY 14225-0400
1	General Electric Company Armament Systems Department ATTN: J. Mandzy 128 Lakeside Avenue Burlington, VT 05401-4985
1	IITRI ATTN: M. J. Klein 10 W. 35th Street Chicago, IL 60616-3799
1	Hercules, Inc. Allegheny Ballistics Laboratory ATTN: William B. Walkup P. O. Box 210 Rocket Center, WV 26726
1	Hercules, Inc. Radford Army Ammunition Plant ATTN: J. Pierce Radford, VA 24141-0299
3	Lawrence Livermore National Laboratory ATTN: L-355, A. Buckingham M. Finger L-324, M. Constantino P. O. Box 808 Livermore, CA 94550-0622
1	Olin Corporation Badger Army Ammunition Plant ATTN: F. E. Wolf Baraboo, WI 53913
2	Olin Corporation Smokeless Powder Operation ATTN: E.J. Kirschke A.F. Gonzalez P. O. Box 222 St. Marks, FL 32355-0222

No. of Copies	Organization
1	Paul Gough Associates, Inc. ATTN: Dr. Paul S. Gough 1048 South Street Portsmouth, NH 03801-5423
1	Physics International Company ATTN: Library, H. Wayne Wampler 2700 Merced Street San Leandro, CA 98457-5602
1	Princeton Combustion Research Laboratory, Inc. ATTN: M. Summerfield 475 US Highway One Monmouth Junction, NJ 08852-9650
2	Rockwell International Rocketdyne Division ATTN: BA08, J.E. Flanagan J. Gray 6633 Canoga Avenue Canoga Park, CA 91303-2703
3	Thiokol Corporation Huntsville Division ATTN: D. Flanigan Dr. John Deur Technical Library Huntsville, AL 35807
2	Thiokol Corporation Elkton Division ATTN: R. Biddle Technical Library P. O. Box 241 Elkton, MD 21921-0241
1	Veritay Technology, Inc. ATTN: E. Fisher 4845 Millersport Highway East Amherst, NY 14501-0305
1	Universal Propulsion Company ATTN: H. J. McSpadden Black Canyon Stage 1 Box 1140 Phoenix, AZ 84029

No. of Copies	Organization
1	Battelle Memorial Institute ATTN: Technical Library 505 King Avenue Columbus, OH 43201-2693
1	Brigham Young University Department of Chemical Engineering ATTN: M. Beckstead Provo, UT 84601
1	California Institute of Technology 204 Karman Laboratory Main Stop 301-46 ATTN: F.E.C. Culick 1201 E. California Street Pasadena, CA 91109
1	California Institute of Technology Jet Propulsion Laboratory ATTN: L. D. Strand, MS 512/102 4800 Oak Grove Drive Pasadena, CA 91109-8099
1	University of Illinois Department of Mechanical/Industrial Engineering ATTN: H. Krier 144 MEB; 1206 N. Green Street Urbana, IL 61801-2978
1	University of Massachusetts Department of Mechanical Engineering ATTN: K. Jakus Amherst, MA 01002-0014
1	University of Minnesota Department of Mechanical Engineering ATTN: E. Fletcher Minneapolis, MN 55414-3368
3	Georgia Institute of Technology School of Aerospace Engineering ATTN: B.T. Zinn E. Price W.C. Strahle Atlanta, GA 30332

No. of Copies	Organization
1	Institute of Gas Technology ATTN: D. Gidaspow 3424 S. State Street Chicago, IL 60616-3896
1	Johns Hopkins University Applied Physics Laboratory Chemical Propulsion Information Agency ATTN: T. Christian Johns Hopkins Road Laurel, MD 20707-0690
1	Massachusetts Institute of Technology Department of Mechanical Engineering ATTN: T. Toong 77 Massachusetts Avenue Cambridge, MA 02139-4307
1	Pennsylvania State University Applied Research Laboratory ATTN: G.M. Faeth University Park, PA 16802-7501
1	Pennsylvania State University Department of Mechanical Engineering ATTN: K. Kuo University Park, PA 16802-7501
1	Purdue University School of Mechanical Engineering ATTN: J. R. Osborn TSPC Chaffee Hall West Lafayette, IN 47907-1199
1	SRI International Propulsion Sciences Division ATTN: Technical Library 333 Ravenwood Avenue Menlo Park, CA 94025-3493
1	Rensselaer Ploytechnic Institute Department of Mathematics Troy, NY 12181

No. of Copies	Organization
2	Director Los Alamos Scientific Laboratory ATTN: T3, D. Butler M. Division B. Craig P. O. Box 1663 Los Alamos, NM 87544
1	General Applied Sciences Laboratory ATTN: J. Erdos 77 Raynor Avenue Ronkonkama, NY 11779-6649
1	Battelle PNL ATTN: Mr. Mark Garnich P. O. Box 999 Richland, WA 99352
1	Stevens Institute of Technology Davidson Laboratory ATTN: R. McAlevy, III Castle Point Station Hoboken, NJ 07030-5907
1	Rutgers University Department of Mechanical and Aerospace Engineering ATTN: S. Temkin University Heights Campus New Brunswick, NJ 08903
1	University of Southern California Mechanical Engineering Department ATTN: 0HE200, M. Gerstein Los Angeles, CA 90089-5199
2	University of Utah Department of Chemical Engineering ATTN: A. Baer G. Flandro Salt Lake City, UT 84112-1194
1	Washington State University Department of Mechanical Engineering ATTN: C. T. Crowe Pullman, WA 99163-5201

No. of
Copies Organization

1 Alliant Techsystems, Inc.
ATTN: R. E. Tompkins
MN38-3300
10400 Yellow Circle Drive
Minnetonka, MN 55343

1 Science Applications, Inc.
ATTN: R. B. Edelman
23146 Cumorah Crest Drive
Woodland Hills, CA 91364-3710

1 Battelle Columbus Laboratories
ATTN: Mr. Victor Levin
505 King Ave.
Columbus, OH 43201-2693

1 Hercules, Inc.
Allegheny Ballistics Laboratory
Propulsion Technology Department
ATTN: Mr. Thomas F. Farabaugh
P.O. Box 210
Rocket Center, WV 26726

Aberdeen Proving Ground

Cdr, CSTA
ATTN: STECS-LI, R. Hendricksen

USER EVALUATION SHEET/CHANGE OF ADDRESS

This Laboratory undertakes a continuing effort to improve the quality of the reports it publishes. Your comments/answers to the items/questions below will aid us in our efforts.

1. BRL Report Number BRL-TR-3206 Date of Report February 1991

2. Date Report Received _____

3. Does this report satisfy a need? (Comment on purpose, related project, or other area of interest for which the report will be used.) _____

4. Specifically, how is the report being used? (Information source, design data, procedure, source of ideas, etc.) _____

5. Has the information in this report led to any quantitative savings as far as man-hours or dollars saved, operating costs avoided, or efficiencies achieved, etc? If so, please elaborate. _____

6. General Comments. What do you think should be changed to improve future reports? (Indicate changes to organization, technical content, format, etc.) _____

CURRENT ADDRESS

Name

Organization

Address

City, State, Zip Code

7. If indicating a Change of Address or Address Correction, please provide the New or Correct Address in Block 6 above and the Old or Incorrect address below.

OLD ADDRESS

Name

Organization

Address

City, State, Zip Code

(Remove this sheet, fold as indicated, staple or tape closed, and mail.)

---FOLD HERE---

DEPARTMENT OF THE ARMY
Director
U.S. Army Ballistic Research Laboratory
ATTN: SLCBR-DD-T
Aberdeen Proving Ground, MD 2100[illegible]-5066
OFFICIAL BUSINESS

NO POSTAGE
NECESSARY
IF MAILED
IN THE
UNITED STATES

BUSINESS REPLY MAIL
FIRST CLASS PERMIT No 0001, APG, MD

POSTAGE WILL BE PAID BY ADDRESSEE

Director
U.S. Army Ballistic Research Laboratory
ATTN: SLCBR-DD-T
Aberdeen Proving Ground, MD 21005-9989

---FOLD HERE---